Kuramochi *et al.*
Progress in Earth and Planetary Science (2023) 10:69
https://doi.org/10.1186/s40645-023-00598-4

Progress in Earth and Planetary Science

RESEARCH ARTICLE

Open Access

Coherent amplification of the Okhotsk high, Korean trough, and northwestern Pacific subtropical high during heavy rainfall over Japan in August 2021

Masaya Kuramochi[1*], Hiroaki Ueda[2], Tomoshige Inoue[2], Meiji Honda[3] and Koutarou Takaya[4]

Abstract

In August 2021, rain front stagnation in Japan resulted in prolonged and disastrous rainfall across the entire country. During the heavy rainfall period, the large-scale atmospheric field over the East Asian–western North Pacific region was characterized by meridional tripolar circulation anomalies: the Okhotsk high (OH), the trough over the Korean Peninsula (Korean trough), and the northwestern Pacific subtropical high (NWPSH). Simultaneously, tropical convective activity was enhanced over the eastern Indian Ocean and suppressed over the tropical western–central Pacific. This study investigates the dynamic mechanism of linkage of the extratropical tripolar anomalies and the effects of tropical convective modulation using a reanalysis dataset, a cutoff low detection scheme, the potential vorticity inversion method, and numerical experiments. Upper-tropospheric blocking over eastern Siberia connected to the surface OH is conducive to the stagnation of synoptic depressions, including cutoff lows and troughs, over the Korean Peninsula, contributing to the development and maintenance of the quasi-stationary Korean trough. Rossby waves emanating from the Korean trough excite an anticyclonic anomaly over the northwestern Pacific. This upper-level anomalous anticyclone acts to enhance the surface NWPSH through zonal heat transport, accompanied by a northward tilting structure with height. Simultaneously, the tropical intraseasonal oscillation is amplified over the Indo–western Pacific Ocean sector under the negative-phase Indian Ocean dipole and multi-year La Niña conditions. The combination of enhanced convection over the eastern Indian Ocean and suppressed convection across the tropical western–central Pacific reinforces the NWPSH. The anomalous circulation associated with the extratropical tripolar pattern and concurrent tropical heat forcing causes more moisture transport, convergence, and anomalous ascent, which contribute to heavy rainfall in Japan. These results suggest that the dynamically correlated amplification of tropical and extratropical circulation anomalies plays a crucial role in precipitation variability in East Asia.

Keywords Heavy rainfall, Climate variability, East Asian summer monsoon, Rossby wave propagation, Intraseasonal oscillation, Northwestern Pacific subtropical high, Korean trough, Okhotsk high, Cutoff low, Tropical–extratropical interaction

*Correspondence:
Masaya Kuramochi
kuramochi.masaya.sp@alumni.tsukuba.ac.jp
Full list of author information is available at the end of the article

1 Introduction

During the late boreal summer of 2021, the Japanese islands recorded extremely heavy rainfall associated with the stagnation of a rain front, which resulted in disastrous floods in central Japan as well as the Kyushu region (western Japan) (Japan Meteorological Agency [JMA] 2021). As shown in Fig. 1a, the time series of observed precipitation in Japan indicates continued wet conditions in August 2021. Although the early summer rainy season in mainland Japan, known as Baiu, is generally in June–July (e.g., Yoshino 1965; Akiyama 1973; Ueda et al. 2009; Sampe and Xie 2010), precipitation in August 2021 was remarkable in comparison with that during Baiu in the same year (Fig. 1a). Figure 1b and 1c shows the spatial distributions of the precipitation anomalies relative to the climatological mean during the heavy rainfall period (August 5–20, 2021). Enhanced precipitation extended over South China, the East China Sea, and Japan. This zonally elongated precipitation anomaly appeared to be similar to the Meiyu–Baiu rain front, which is climatologically more prominent in early summer than in late summer. The western side of Japan recorded four times more precipitation than the climatological average in mid-August (Fig. 1a and c). The occurrence of mesoscale quasi-stationary linear precipitation systems was reported in the Kyushu region during this heavy rainfall event (JMA 2021).

From the viewpoint of the global climate system, several atmospheric and oceanic anomalies have been identified as contributing factors to recent heavy rainfall events in East Asia during summer (e.g., Shimpo et al. 2019; Takemura et al. 2019; Takaya et al. 2020; Harada et al. 2020; Horinouchi et al. 2021; Ueda et al. 2021; Park et al. 2021a; Chen et al. 2022). They can be broadly classified into two aspects: effects from the tropics and extratropics. With regard to the effect of tropical modulation, anomalous sea surface temperatures (SSTs) and/or convective heating over the Indo–western Pacific sector induce an enhancement of the northwestern Pacific subtropical high (NWPSH) in the lower troposphere (Lu 2001; Terao and Kubota 2005; Wu et al. 2010; Wang et al. 2013; Takaya et al. 2020; Ueda et al. 2021), thereby

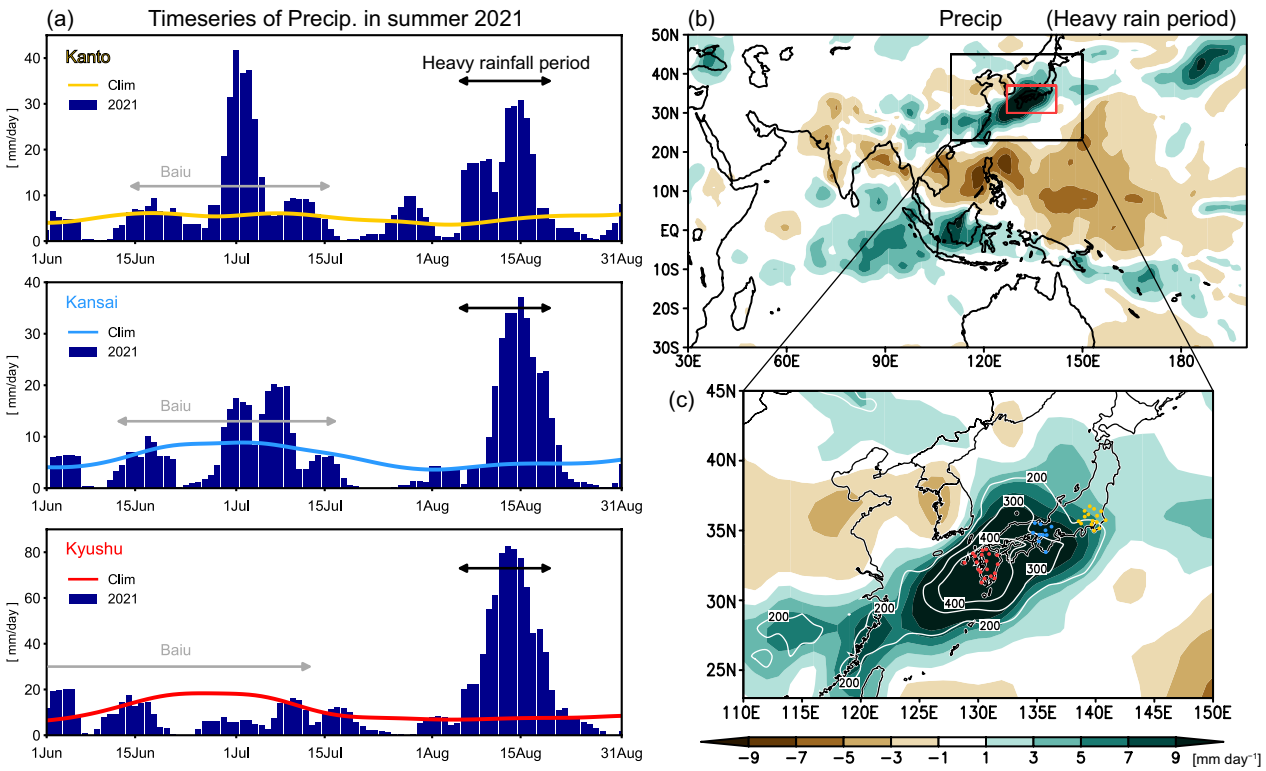

Fig. 1 Precipitation in East Asia during the summer of 2021. **a** Time series of observed precipitation (blue bar; unit: mm day^{-1}) in Kanto (top panel), Kansai (middle panel), and Kyushu (bottom panel), Japan by AMeDAS. Color lines indicate their climatological mean for 1991–2020. Gray and black two-way arrows in each panel denote the Baiu period defined by the JMA and the heavy rainfall period in this study [August 5–20, 2021], respectively. **b**, **c** Spatial distributions of period-averaged precipitation anomaly (shading; unit: mm day^{-1}) as deviation from the climatological mean during the heavy rainfall period. Red rectangle in **b** is the region of area-averaged precipitation over Japan [30°–37°N, 127°–142°E]. In **c**, white contours indicate ratios of precipitation to its climatological mean (unit: %), and color dots are plotted at the location of the AMeDAS observation stations in Kanto (yellow), Kansai (blue), and Kyushu (red) used for showing the time series in (**a**)

allowing more moisture to be transported from the tropics to East Asia (Chowdary et al. 2013; Kamae et al. 2017; Sekizawa et al. 2019). The El Niño–Southern oscillation (ENSO), particularly its phase transition from mature El Niño in the preceding boreal winter, affects the excitation of the anomalous NWPSH and the resultant precipitation variability in East Asia (Chang et al. 2000; Wang et al. 2000, 2001; Tomita et al. 2004; Naoi et al. 2020). Wang et al. (2000) indicated a local effect of concurrent SST cooling in the tropical western Pacific associated with El Niño in the preceding winter on the intensified NWPSH. In addition, subsequent studies showed that the sequential process and its remote effect involve the Ekman divergence associated with the eastward-propagating Kelvin wave forced by the warm Indian Ocean capacitor (Yang et al. 2007; Xie et al. 2009) and positive feedback from the anomalous NWPSH through the wind-evaporation-SST feedback mechanism (Kawamura et al. 2001; Du et al. 2009; Kosaka et al. 2013). This trans-basin air–sea interaction related to the transition from El Niño in the boreal summer is understood as the Indo–western Pacific Ocean Capacitor (IPOC) effect (Xie et al. 2016). However, Wang et al. (2013) suggested that SST cooling in the equatorial central Pacific, i.e., summer La Niña-like conditions, can intensify the NWPSH. Observational evidence has consistently shown that La Niña events are concurrent with extremely wetter conditions in East Asia, such as in summer 1988 (Nitta 1990), June–July 2020 (Ueda et al. 2021; Park et al. 2021a), and late summer 2021 (see Sect. 3.1).

In the meanwhile, the Rossby wave trains associated with the meandering of the extratropical westerly jet have also been interpreted as significant contributors to precipitation variability in East Asia (Wakabayashi and Kawamura 2004; Kosaka et al. 2011; Hirota and Takahashi 2012; Chen and Huang 2012; Harada et al. 2020; Horinouchi et al. 2021). For example, the quasi-stationary wave train along the Asian jet centered at approximately 40°N, called the Silk Road pattern (Enomoto et al. 2003), is crucial for enhancing and maintaining perturbation vortices through energy propagation and conversion (Enomoto 2004; Sato and Takahashi 2006; Kosaka et al. 2009). The deepened upper-level trough near the Korean Peninsula acts to dynamically produce vertical motion accompanied by heavy rainfall in Japan and Korea (Takemura et al. 2019; Tsuji et al. 2020; Yokoyama et al. 2020; Park et al. 2021b). Moreover, a cold cutoff low or trough emerges around East Asia simultaneously with the occurrence of heavy rainfall (Ninomiya and Shibagaki 2007; Zhao and Sun 2007; Shimpo et al. 2019). Harada et al. (2020) showed that the formation of an upper-level trough over the Korean Peninsula during a heavy rain event in July 2018 was dominated by high-frequency (shorter than 8 days) variability. Furthermore, the Okhotsk high (OH), which is one of the major climate systems during the Baiu season, is an essential factor in maintaining the rain front over East Asia because it transports cold air masses (Ninomiya and Mizuno 1985; Yim et al. 2014). The development of the surface OH is closely related to the meandered polar front jet centered at ~ 60°N in the upper troposphere as well as the land–sea thermal contrast (Nakamura and Fukamachi 2004; Tachibana et al. 2004; Sato and Takahashi 2007). Kawasaki et al. (2021) suggested the role of the cold Okhotsk Sea in the enhancement of the NWPSH and Baiu rain front by increasing the baroclinic instability controlled by the meridional temperature gradient.

Although the primary factors causing heavy and prolonged rainfall over East Asia have been extensively investigated from the tropical and extratropical perspectives, their dynamic relationships have not been sufficiently discussed. Kosaka et al. (2011) showed that several teleconnection patterns, such as ENSO, the Pacific–Japan pattern (Nitta 1987), the Silk Road pattern, and the wave train along the polar front jet accompanied by the surface OH, coherently contribute to summertime precipitation variability in East Asia. Moreover, by performing singular value decomposition analysis, Hirota and Takahashi (2012) showed that a meridional tripolar pattern of circulation anomalies appears over the Philippines, China/Japan, and eastern Siberia, causing anomalous precipitation in East Asia. They indicated that the tripolar anomaly pattern was accompanied by internal wave propagation and tropical diabatic heating. These pioneering studies suggest the presence of a dynamically linked tropical–extratropical covariability that causes heavy rainfall in the northwestern Pacific during summer.

This study investigates the anomalous circulation fields associated with heavy rainfall over Japan that occurred in August 2021, focusing on the tropical–extratropical relationship. To explain the atmospheric circulation anomalies in August 2021, various aspects of the circulation anomalies must be considered, including Rossby wave-packet propagation, Rossby wave breaking, interactions between the upper- and lower-level circulations, and tropical heat forcing. The remainder of this paper is structured as follows: In Sect. 2, the data and methods used in our analyses are explained. Section 3.1 presents the observed climate anomalies in the tropics and extratropics in August 2021. Section 3.2 presents analyses of the relationships between (1) the Rossby wave breaking over eastern Siberia and trough over the Korean Peninsula, and (2) the upper- and lower-level circulations in the NWPSH region. Section 3.3 discusses the roles of tropical heat forcing. In Sect. 4, the conclusions are presented.

2 Data and methods

This section presents the data and tools used for the analyses from various tropical and extratropical perspectives, including Rossby wave propagation/breaking, movement of upper-level depressions, vertical circulation interactions, and tropical heat forcing.

2.1 Observational data

The atmospheric data used in this study were 6-hourly data from the Japanese 55-year Reanalysis (JRA-55) dataset with a horizontal resolution of 1.25° and 37 pressure levels (Kobayashi et al. 2015) from 1991 to 2021. Additionally, monthly-mean SST data from the Centennial in situ Observation-Based Estimate-SST (COBE-SST) with a horizontal resolution of 1.0° (Ishii et al. 2005) were used for the same period. For daily precipitation data, we utilized the Global Precipitation Climatology Project (GPCP) dataset with a horizontal resolution of 1.0° (Huffman et al. 2001) for the period of 1997–2021 from the National Oceanic and Atmospheric Administration (NOAA). Precipitation observations in Japan were obtained from a data source based on the automated meteorological data acquisition system (AMeDAS) maintained by the JMA. Tropical convective activity was quantified using the daily interpolated outgoing longwave radiation (OLR) data with a horizontal resolution of 2.5° (Liebmann and Smith 1996) provided by NOAA for the period of 1991–2021. We also used the Madden–Julian oscillation (MJO) daily index provided by the Australian Bureau of Meteorology as the real-time multivariate MJO (RMM) index (Wheeler and Hendon 2004) and the boreal summer intraseasonal oscillation (BSISO) daily index (Lee et al. 2013) provided by the Asia–Pacific Economic Cooperation (APEC) Climate Center.

We mainly analyzed the anomalous climate fields during the heavy rainfall period (August 5–20, 2021; Fig. 1a). The 6-hourly and daily data from JRA-55 and GPCP, respectively, were temporally averaged for the period, and the climatological-mean state was defined as the study period average for the same calendar day of each dataset. Anomalies were defined as deviations from the climatological mean. No long-term detrending was applied.

2.2 Wave-activity flux

The propagation of stationary Rossby waves was analyzed using the quasi-geostrophic (QG) wave-activity flux defined by Takaya and Nakamura (2001). The horizontal component of flux $\mathbf{W}$ is defined as follows:

$$W = \frac{p^*}{2\sqrt{\overline{u}^2+\overline{v}^2}}\begin{pmatrix} \overline{u}\left(\psi'^2_x - \psi'\psi'_{xx}\right) + \overline{v}\left(\psi'_x\psi'_y - \psi'\psi'_{xy}\right) \\ \overline{u}\left(\psi'_x\psi'_y - \psi'\psi'_{xy}\right) + \overline{v}\left(\psi'^2_y - \psi'\psi'_{yy}\right) \end{pmatrix}, \tag{1}$$

where the overbar and prime denote the climatological-mean state and anomaly, respectively, u is the zonal wind, v is the meridional wind, $\psi = \phi/f_0$ is the geostrophic streamfunction, with ϕ as the geopotential and f_0 as the reference Coriolis parameter, and p^* =(pressure/1000 hPa). Subscripts x and y denote the partial derivatives with respect to longitude and latitude, respectively. The flux $\mathbf{W}$ is proportional to the group velocity of stationary Rossby waves in the plain wave limit; therefore, it is a useful diagnostic tool for depicting the wave-packet propagation of Rossby waves in applications to the data. The wave activity is also transported by the phase speed of the wave (Takaya and Nakamura 2001), but the phase-speed term was omitted here under the assumption of quasi-stationary Rossby waves.

2.3 Cutoff low index

To detect synoptic depressions in the mid- to upper troposphere including cutoff lows and preexisting troughs, the cutoff low index (COL index; Kasuga et al. 2021) was utilized, which is a useful tool for seamless detection of isobaric depressions. This scheme was based on the geometric horizontal slope of the geopotential height field. The average slope (AS) function representing the two-dimensional average of the four-directional slope is defined as follows:

$$\begin{aligned} \mathrm{AS}(x,y;r) = &\frac{1}{4r}\big[Z(x+r,y) + Z(x-r,y) \\ &+Z(x,y+r) + Z(x,y-r) - 4Z(x,y)\big], \end{aligned} \tag{2}$$

where x and y denote the longitudinal and latitudinal grid points, respectively, r is the radial searching variable, and Z is the geopotential height at any isobaric level. Here, the AS maximum against variable r is denoted as AS^+, that is

$$\mathrm{AS}^+(x,y) \equiv \max_r \mathrm{AS}(x,y;r), \tag{3}$$

and the bottom points of a geometric depression (x_b, y_b) are specified by the local maximum of AS^+ as follows:

$$S_o \equiv \mathrm{AS}^+(x_b,y_b) = \mathrm{AS}(x_b,y_b;r_o) \geq \mathrm{AS}(x,y;r), \tag{4}$$

where S_o is the optimal slope, and r_o is the optimal radius. Hence, AS^+ represents the depression of the geopotential height field, S_o reflects the strength and position of the cutoff lows or toughs, and r_o is interpreted as their depression area. When a local height minimum point is located within the optimal radius of a detected depression, it is regarded as a cutoff low; otherwise, it is

regarded as a trough. Based on the definition of the AS function [Eq. (2)], the AS minimum (AS^-) may detect anticyclonic disturbances including blocking highs and ridges (Kasuga et al. 2021). The COL index was calculated using the 6-hourly geopotential height data from JRA-55.

2.4 Quasi-geostrophic potential vorticity inversion

The dynamic relationship between the upper- and lower-tropospheric circulation anomalies was determined using the potential vorticity (PV) inversion technique. In the QG framework, PV (q; QGPV) is given by:

$$q = f + \nabla^2\psi + \frac{\partial}{\partial p}\left(\frac{f_0^2}{\sigma}\frac{\partial \psi}{\partial p}\right), \tag{5}$$

and anomalous QGPV (q') is written as:

$$q' = \nabla^2\psi' + \frac{\partial}{\partial p}\left(\frac{f_0^2}{\sigma}\frac{\partial \psi'}{\partial p}\right) = \mathcal{L}_g(\psi'), \tag{6}$$

where f is the planetary vorticity, $\sigma \equiv -RT_0p^{-1}\mathrm{d}\ln\theta_0/\mathrm{d}p$ is the static stability, with R as the gas constant and θ_0 as the potential temperature corresponding to the basic state temperature T_0, and $\mathcal{L}_g = \nabla^2 + (\partial/\partial p)\left[\left(f_0^2/\sigma\right)(\partial/\partial p)\right]$ is the linear operator. Using the PV invertibility (Charney and Stern 1962; Hoskins et al. 1985), the distribution of the anomalous streamfunction (ψ') is uniquely determined from a specified perturbation PV (q') by inverting the Laplacian-like operator ($\mathcal{L}_g$), i.e., $\psi' = \mathcal{L}_g^{-1}(q')$. Appropriate boundary conditions are required to solve the Laplacian inversion problem (Bretherton 1966; Hoskins et al. 1985). To invert upper-tropospheric QGPV anomalies, Nakamura and Fukamachi (2004) and Takaya and Nakamura (2005) performed an inversion with an imaginary flat surface much deeper than the actual ground surface, which allowed the immediate effect of the upper level on the ground surface to be extracted. The climatological Brunt–Väisälä frequency-averaged zonally at each pressure surface was assigned, and the perturbation potential temperature (θ') was set to zero at the imaginary surface as the lower-boundary condition. The same measures were adopted in this study. We refer to Takaya and Nakamura (2005) for details on our QGPV inversion method.

2.5 Linear baroclinic model

To assess the effects of tropical diabatic heating on the anomalous NWPSH, we used the linear baroclinic model (LBM; Watanabe and Kimoto 2000), which is a spectral model based on linearized primitive equations. The LBM used in this study comprised 20 sigma levels with a horizontal resolution of T42 and employed del-forth horizontal diffusion, Rayleigh friction, and Newtonian thermal damping. The e-folding decay time of the diffusion coefficient was set to 6 h for the maximum horizontal wavenumber. The damping coefficient was set to half a day for the lowest three levels, one day for the uppermost two levels, and 20 days elsewhere. The LBM was forced with externally imposed heating and time integrated to a steady state, which was day 15 when the model reached a quasi-steady state in this study. Details regarding the experimental settings, including the prescribed heating and background states, are presented in Sect. 3.3.1.

3 Results and discussion

3.1 Anomalous fields during the heavy rainfall period in August 2021

3.1.1 Climate anomalies in the atmosphere and ocean

The anomalous atmospheric circulation fields during the heavy rainfall period in August 2021 are shown in Fig. 2. The sea-level pressure (SLP) field exhibited positive anomalies over the subtropical western Pacific and Okhotsk Sea (Fig. 2a), which were identified as the intensified NWPSH and OH, respectively. A zonally elongated negative SLP anomaly was found over Japan between the two intensified anticyclones, corresponding to an enhanced rain band (Fig. 1b). The anomalous moisture flux in the lower troposphere indicated that the intensified NWPSH transported more moisture to the extratropics and converged over Japan (Fig. 2b), resulting in heavy rainfall. The anomalous OH and associated northerly winds can contribute to moisture flux convergence anomaly, which favors the frontal zone. In the mid-troposphere (500 hPa), a meridional tripolar structure comprising an anticyclonic anomaly over eastern Siberia, an anomalous trough over the Korean Peninsula (hereinafter referred to as the Korean trough), and an anticyclone appearing southeast of the Japan region was evident (Fig. 2a). The northern anticyclonic anomaly extended over eastern Siberia toward the Okhotsk Sea, where blocking events occur frequently during boreal summer (e.g., Barriopedro et al. 2006). It is important to note that the Korean trough as well as the blocking-like anticyclonic anomaly over eastern Siberia were quasi-stationary systems, as discussed in Sect. 3.2.1. The other anticyclonic circulation anomaly over the subtropical northwestern Pacific appeared to correspond to the enhancement of the surface NWPSH, whereas the anomalous circulation at 500 hPa was located slightly northeast of the surface anomalies. The vertical structure of the northward tilting with height is discussed in Sect. 3.2.2.

The upper-tropospheric circulation anomalies show a wave-train pattern from northern Europe via Central Asia to Japan (Fig. 2c). The wave train over the Eurasian continent was accompanied by an eastward wave-activity flux along the Asian jet, indicating the propagation of

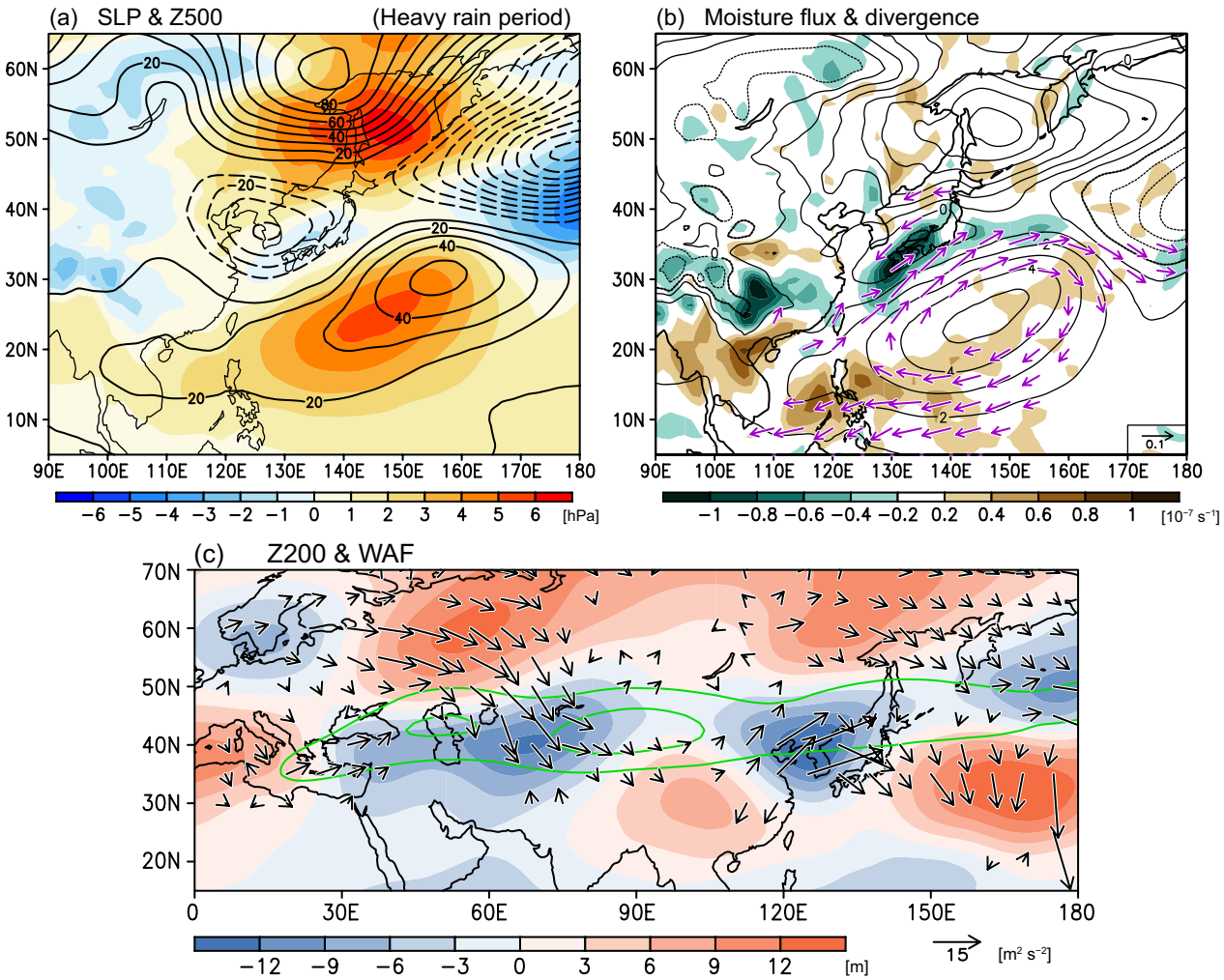

Fig. 2 Anomalous atmospheric fields during the heavy rainfall period in August 2021. **a** Anomalies of SLP (shading; unit: hPa) and geopotential height at 500 hPa (contours; unit: m). **b** Moisture flux anomaly (vectors; unit: kg kg^{-1} m s^{-1}) at 925 hPa and its divergence (shading; unit: s^{-1}). SLP anomaly (unit: hPa) is superimposed by thin contours. **c** Geopotential height anomaly at 200 hPa (shading; unit: m) and wave-activity flux (vectors; unit: m^2 s^{-2}). Green contours indicate 20 and 30 m s^{-1} isolines of the climatological-mean zonal winds at 200 hPa

stationary Rossby waves. The Korean trough appeared to be the easternmost wave train over the continent; however, the eastward propagation was obscure around southern China (100°E). Moreover, in the western North Pacific, the wave-activity flux appeared to emanate from the deepened Korean trough to the anticyclone over the subtropical western Pacific in a southeastward direction. These extratropical atmospheric features, which indicated the occurrence of the OH/blocking, Korean trough, and NWPSH, resembled to the modulated circulation fields associated with the previous heavy rainfall events over East Asia in July 2018 (e.g., Shimpo et al. 2019; Harada et al. 2020) and July 2020 (Park et al. 2021a).

Figure 3 shows the SST anomalies in August 2021 and the temporal evolution of the tropical oceanic indices based on the area-averaged SST anomalies. The negative SST anomalies in the eastern side of the equatorial Pacific and the positive anomalies in the tropical western Pacific indicate La Niña conditions in August 2021 (Fig. 3a). Simultaneously, SST in the eastern Indian Ocean was higher than normal, which coincided with cooling in the western Indian Ocean. This SST pattern in the Indian Ocean was identified as a negative phase of the Indian Ocean dipole (IOD). The time series of the Niño3.4 index shows continued La Niña conditions from the previous winter of 2020/21 through the summer of 2021 to the next winter of 2021/22 (Fig. 3b; World Meteorological Organization 2022), whereas the negative-phase IOD emerged from May 2021 (Fig. 3b).

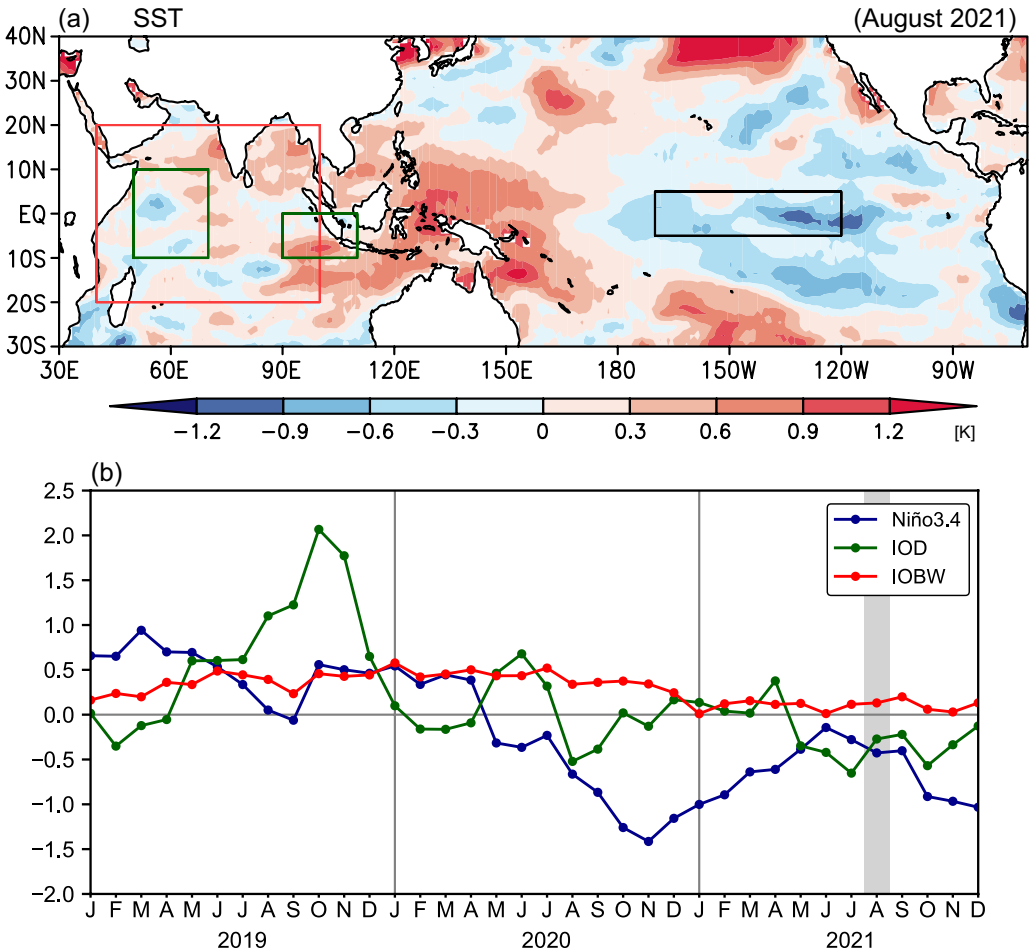

Fig. 3 **a** SST anomalies (unit: K) in August 2021. **b** Monthly time series of the tropical oceanic indices from 2019 to 2021: Niño3.4 index (blue line) as [5°S–5°N, 170°–120°W] (Trenberth 1997), Indian Ocean dipole (IOD) index (green line) as the difference between [5°S–5°N, 50°–70°E] and [10°S–Equator, 90°–110°E] (Saji et al. 1999), and Indian Ocean basin warming (IOBW) index (red line) as [20°S–20°N, 40°–100°E]. The units are K. The areas of the indices are shown by rectangles in (**a**)

Regarding the relationship between tropical SST and convection anomalies (Fig. 1b), the anomalously high SST around the Maritime Continent was consistent with the in situ enhancement of convective activity. Several studies have shown that significantly suppressed convection over the equatorial central Pacific appears in La Niña summers associated with the modulated Walker circulation (e.g., Webster and Yang 1992; Ju and Slingo 1995). The thermodynamic relationship between the anomalous NWPSH and diabatic heating over the Indo–Pacific sector is discussed in Sect. 3.3.

3.1.2 Synchronized amplification of climate anomalies

The previous subsection presented the time-mean anomalies in the atmosphere and ocean during the heavy rainfall period in August 2021. This subsection focuses on the daily evolution of these key factors. Figure 4 shows the daily time series of the indices representing the intensity of the anomalous circulation and precipitation in August 2021. The upper-level blocking high over eastern Siberia (pink lines) and surface OH (red lines) varied coherently, indicating their strong linkage as shown by Nakamura and Fukamachi (2004). The intensity of the blocking high and OH reached a maximum on August 8–10, 2021, prior to the maximum precipitation in Japan (August 13, 2021; navy bars). The Korean trough (yellow lines) deepened toward the peak of precipitation in Japan and maintained its intensity for several days. Similarly, the NWPSH (blue lines) intensified in early August and reached its maximum intensity on August 13, 2021. Furthermore, convection over the eastern Indian Ocean was much enhanced in early August and continued during the heavy rainfall period. This synchronized amplification of the OH/blocking, Korean trough, NWPSH, and convective activity over the Indian Ocean

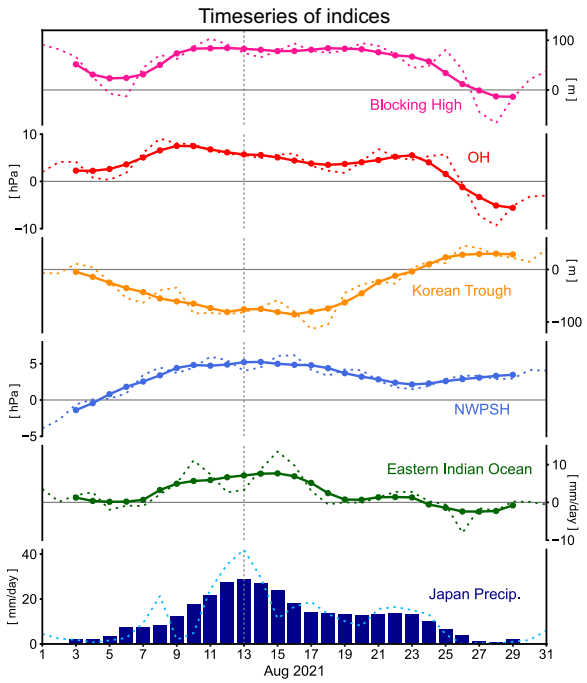

Fig. 4 Daily time series of the indices of the blocking high over eastern Siberia (pink), Okhotsk high (OH; red), Korean trough (yellow), northwestern Pacific subtropical high (NWPSH; blue), convective activity over the eastern Indian Ocean (green), and precipitation in Japan (heavy blue bar) in August 2021. Dotted and solid lines indicate the daily and 5-day running means, respectively. The bottom bars also indicate the 5-day running mean. Vertical dotted lines denote August 13, 2021. The indices were defined by area average as follows; Blocking high: Geopotential height anomaly at 500 hPa (unit: m) over eastern Siberia [50°–60°N, 125°–140°E], OH: SLP anomaly (unit: hPa) over the Okhotsk Sea [45°–60°N, 140°–155°E], Korean trough: Geopotential height anomaly at 500 hPa (unit: m) over the Korean Peninsula [30°–45°N, 120°–135°E], NWPSH: SLP anomaly (unit: hPa) over the subtropical northwestern Pacific [15°–30°N, 130°–155°E], Convective activity: Precipitation anomaly (unit: mm day^{-1}) over the eastern Indian Ocean [5°S–10°N, 85°–100°E], Japan precipitation: Precipitation (unit: mm day^{-1}) over Japan [30°–37°N, 127°–142°E]. Precipitation was based on the GPCP data

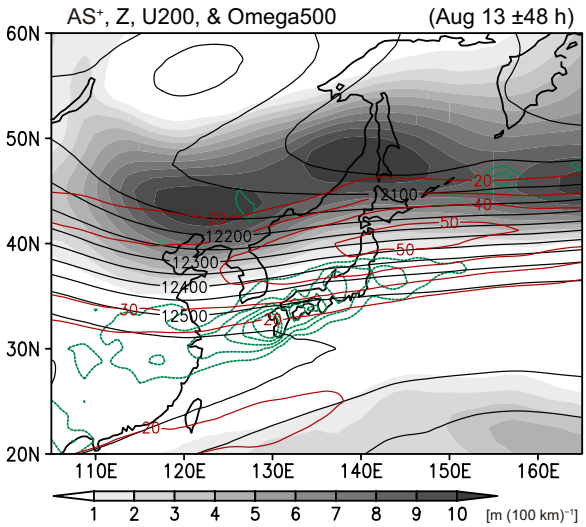

Fig. 5 Spatial distributions of the mean atmospheric fields in August 11–15, 2021. AS^{+} (shading; unit: m [100 km]$^{-1}$) and geopotential height (black contours; unit: m) at 200 hPa. Green contours indicate vertical *p*-velocity at 500 hPa from −0.5 to −0.1 Pa s^{-1} with an interval of 0.1 Pa s^{-1}. The 200-hPa horizontal wind velocity more than 20 m s^{-1} is superimposed by red contours with an interval of 10 m s^{-1}

implies a dynamic linkage in the tropical–extratropical atmosphere. Therefore, we attempt to explain the synchronicity in the following sections.

3.2 Dynamical mechanisms of tripolar circulation synchronicity

3.2.1 Trough over the Korean Peninsula and blocking high over eastern Siberia

The previous section described the coherent amplification of the tripolar circulation anomalies. In this subsection, the relationship between the quasi-stationary Korean trough and the eastern Siberian blocking high is analyzed using the COL index. Although the stationary cyclonic anomaly and related high-frequency variability over the Korean Peninsula have been suggested as important contributors to a heavy rainfall event in western Japan (Harada et al. 2020), the specific behavior of the shorter-scale eddies has not been explicitly shown. Therefore, the detection of synoptic-scale isobaric depressions using the COL index might be advantageous for capturing the motions of upper-level transient eddies and clarifying the formation of the quasi-stationary Korean trough.

The spatial distributions of the upper-tropospheric geopotential height and AS^{+} around the day of the rainfall peak are shown in Fig. 5. Positive values of AS^{+} (gray shading) represent the presence of isobaric depressions corresponding to a deepened trough over northeastern China toward the southern Okhotsk Sea. Moreover, the northward positive gradient of the geopotential height indicates that the trough was accompanied by anticyclonic wave breaking and a blocking high over eastern Siberia. In the southeast of the wave breaking, the salient ascent was found over Japan, south of the jet streak entrance. This strong vertical motion over Japan may be partly attributed to a dynamically induced ascent under the QG balance, as diagnosed using the *Q*-vector proposed by Hoskins et al. (1978) (Additional file 1: Fig. S1). In general, from the perspective of the QG omega equation, the ascent is dynamically required in the south of the upper-tropospheric jet entrance (Hoskins et al. 1987;

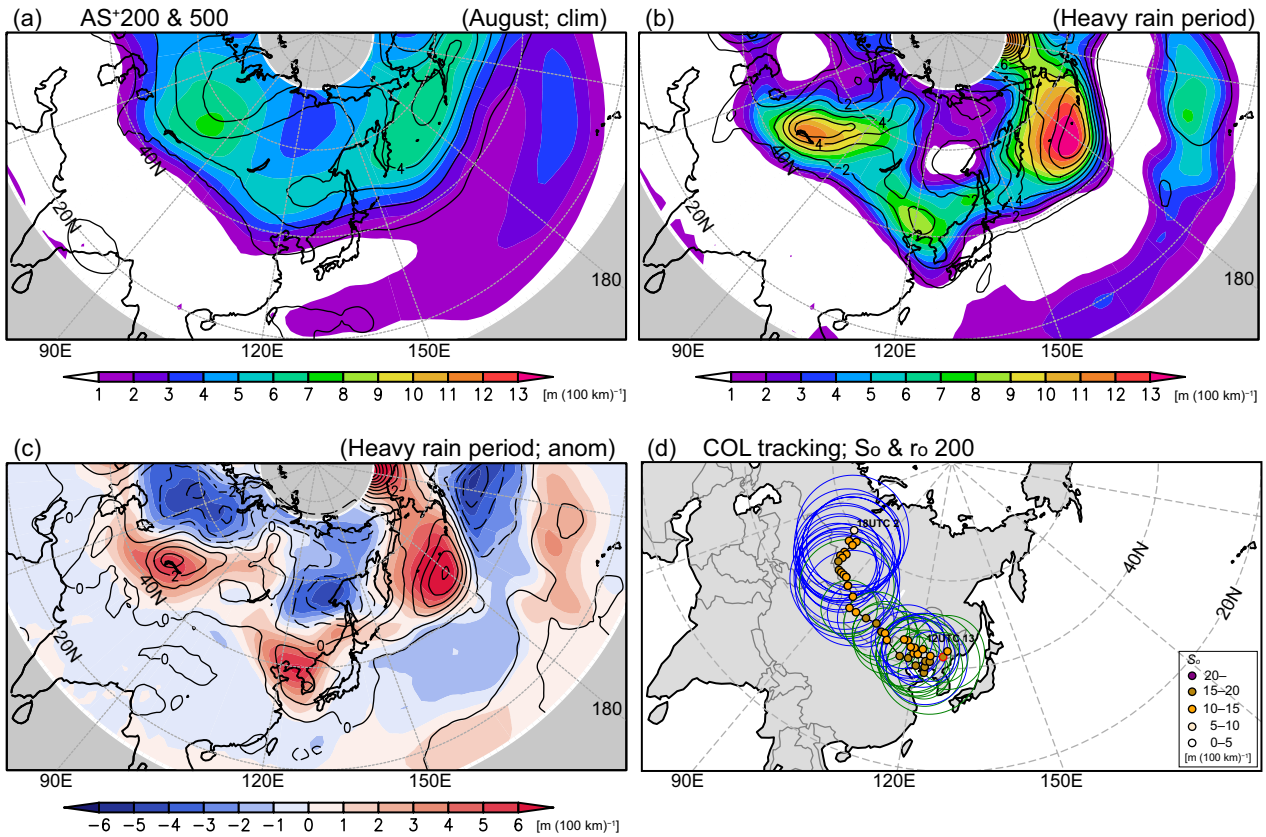

Fig. 6 Spatial distributions of the COL index. Mean AS^+ at 200 hPa (shading) and 500 hPa (contours) in the **a** August climatology and **b** heavy rainfall period in August 2021. **c** Anomalies of AS^+ at 200 hPa (shading) and 500 hPa (contours) during the heavy rainfall period. **d** Tracking of the extracted depression at 200 hPa from development (18 UTC on August 2, 2021) to disappearance (12 UTC on August 13, 2021) with 6-hourly intervals. Color dots represent positions and optimal slope S_o of the depression. Green and blue circles denote optimal radius r_o (unit: km) when the depression was trough and cutoff low, respectively. The units of AS^+ and optimal slope are m $(100\ km)^{-1}$

Park et al. 2021b). Consistent with this fact, Fig. 5 actually shows that the distribution of the intense ascent over Japan was located southwest to the upper-level jet core (>50 m s^{-1}). Moreover, the equatorward Q-vectors were zonally convergent along the jet entrance (Additional file 1: Fig. S1), indicating the presence of the dynamically induced ascent corresponding to the heavy rainfall region.

Figure 6a and b shows the time-mean COL index in the August climatology and the heavy rainfall period in August 2021, respectively. In the August climatology, the AS^+ maxima appeared around Central Asia, Northeast Asia, and the Aleutian Islands (Fig. 6a). The southwestward extension of AS^+ to the subtropical Pacific at 200 hPa corresponds to the so-called tropical upper-tropospheric trough or mid-Pacific trough associated with Rossby wave breaking (Postel and Hitchman 1999; Abatzoglou and Magnusdottir 2006). The climatological-mean AS^+ may imply the main routes and generation areas of cutoff lows from western Siberia via northern East Asia to the Aleutian Islands in the boreal summer. During the rainy period in August 2021 (Fig. 6b), intense AS^+ maxima were found around over Lake Balkhash (45°N, 75°E), the northwest of the Korean Peninsula, and the Aleutian Islands both at 500 and 200 hPa, which were almost the same areas as those of the climatological maxima and exhibited corresponding positive anomalies (Fig. 6c). The geographical locations of the maxima of AS^+ and its anomalies differed slightly. A positive AS^+ anomaly indicated an increase in the frequency and/or intensity of depression. Notably, positive AS^+ anomalies were accompanied by negative AS^+ anomalies in the north. The anomaly of AS^+ corresponded well with that of the upper-level geopotential height (Fig. 2c).

Figure 7 shows distributions of AS^- provided in the COL index denoting bumps on the isobaric surface during the heavy rain period. Overall, the mean AS^- and its anomaly were opposite to those of AS^+ (comparison between Figs. 6 and 7). The maximum and positive anomaly of AS^- over the northern part of eastern Siberia

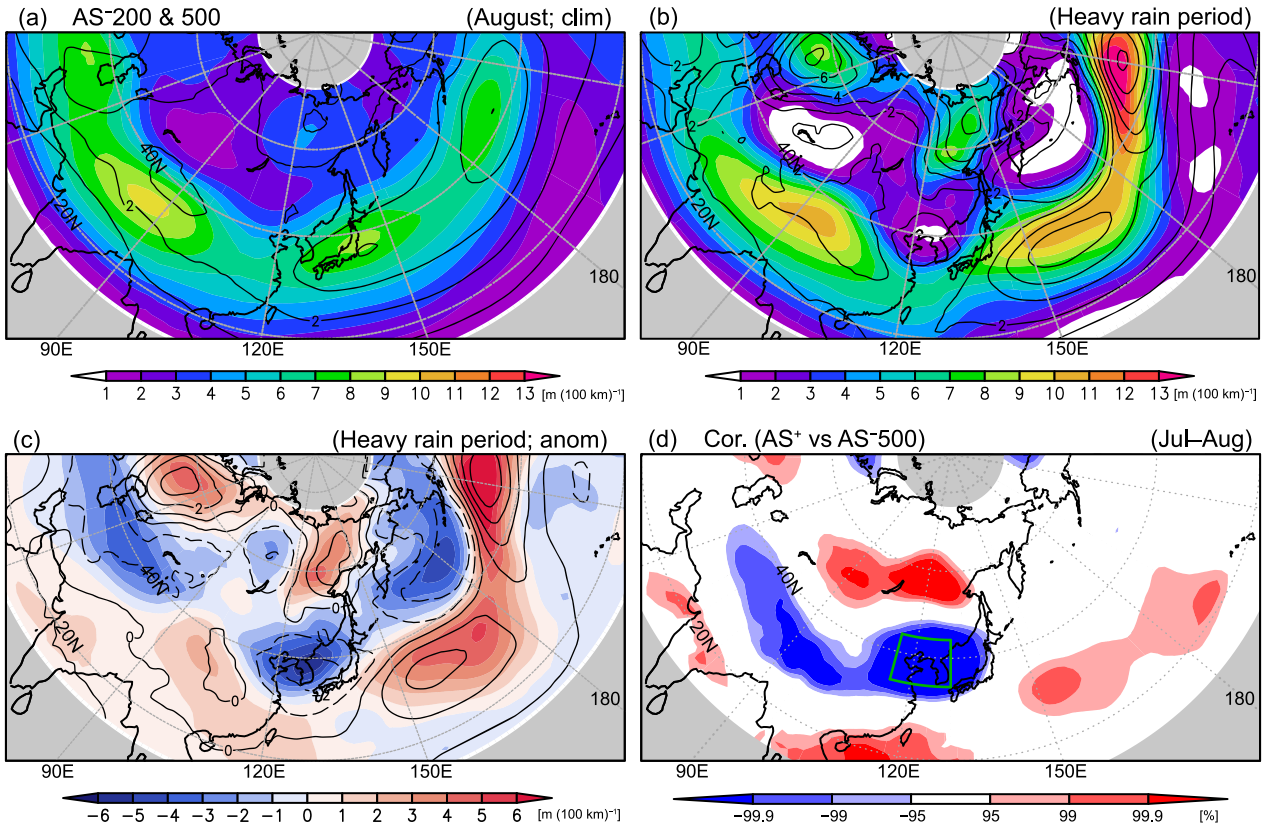

Fig. 7 **a**, **b**, **c** Same as Fig. 6a, b, c, respectively, but for AS^{-}. **d** Spatial distribution of correlation coefficient between monthly-mean AS^{-} and area-averaged AS^{+} near the Korean Peninsula [30°–45°N, 120°–135°E] (green box). Gradational red and blue shadings denote, respectively, positive and negative correlations exceeding the 95, 99, and 99.9% confidence levels. The statistical period was July and August for 1991–2020

represents the occurrence of blocking (Fig. 7b, c). Interestingly, we can find an AS^{-} maximum and a blocking structure over eastern Siberia also in the climatological-mean field in August (Fig. 7a), indicating the frequent occurrence and favorable conditions for blocking. The north–south pair of AS^{-} over eastern Siberia and AS^{+} over the Korean Peninsula implies a classical relationship between blocking highs and lows; in other words, blocking highs are occasionally accompanied by cyclones on the equator side (e.g., Rex 1950; Nakamura et al. 1997; Barriopedro et al. 2006). Even if the cyclone does not completely separate from the background stream, troughs intrude south of the blocking highs, as shown in Fig. 5 (e.g., Lejenäs and Økland 1983; Barriopedro et al. 2006). On the basis of this finding, we show the correlation coefficients between the monthly-mean AS^{-} and area-averaged AS^{+} in the vicinity of the Korean Peninsula in Fig. 7d for the statistical period of July–August from 1991 to 2020. The significant positive correlation over eastern Siberia indicates a strong linkage between the eastern Siberian blocking high and the Korean trough. This result implies a significant coherent amplification between the Siberian blocking high and the Korean trough during the heavy rainfall period in August 2021.

From a Lagrangian perspective, the COL index can track upper-tropospheric depressions and indicate their movements (Kasuga et al. 2021). Using the 6-hourly COL index, we visually performed a back-trajectory analysis of the depression at 200 hPa that appeared over the Korean Peninsula on August 13, 2021; its trajectory is shown in Fig. 6d. The target depression emerged at 18 UTC on August 2, 2021, as a cutoff low over western Siberia, which is a region where cutoff lows develop frequently (Fig. 6a). Subsequently, it moved southeastward over East Asia for several days and remained near the Korean Peninsula for approximately four days. When it remained there, some other small depressions were separated from and also merged with it. This was characterized by an eastward movement toward the cyclonic anomaly over the Aleutian Islands (Additional file 1: Fig. S2). The target depression disappeared at 12 UTC (21 Japan Standard Time) on August 13, 2021, and merged with another cutoff low over Sakhalin. These results indicate that the long-lived cutoff low, which was generated ~ 10 days

earlier in western Siberia, traveled southeastward over East Asia and finally contributed to the heavy rainfall in Japan.

Furthermore, the movements of the synoptic depressions may be associated with the blocking over eastern Siberia and may indicate the formation and deepening processes of the stationary Korean trough. From a vortex–vortex interaction perspective, Yamazaki and Itoh (2013a, b) proposed that relatively small perturbations (synoptic eddies) move along the waveguide to a same-polarity large-scale eddy (blocking highs and lows), thereby contributing to the maintenance of blocking by supplying PV. Based on this idea, the synoptic depressions may have selectively traveled and stagnated south of the blocking high over eastern Siberia (Fig. 6d), thereby deepening the preexisting stationary Korean trough during the heavy rainfall period in August 2021. This suggests an interaction between the stationary cyclonic anomaly and transient cyclonic eddies over the Korean Peninsula.

3.2.2 Relationship between the surface NWPSH and upper-level anticyclone

The preceding subsection suggested a correlation between the Siberian blocking and Korean trough. In this section, we further discuss the possible relationship between extratropical wave propagation in the upper troposphere and anomalous NWPSH in the lower troposphere. As mentioned in Sect. 3.1, stationary Rossby waves emanated from the Korean trough toward the anticyclonic anomaly over the western North Pacific in the upper troposphere (Fig. 2c). This indicates that the upper-tropospheric anomalous anticyclone was excited and maintained by wave propagation from upstream. The resultant negative QGPV anomaly over the western North Pacific (Fig. 8a) may have induced anomalous circulation in the lower troposphere (e.g., Hoskins et al. 1985).

To examine the upper-level impacts on surface circulation, the QGPV inversion was conducted as shown in Fig. 8. Figure 8b shows the anomalous geostrophic winds at 1000 hPa induced solely by the 200-hPa QGPV anomaly in the Northern Hemisphere averaged during the heavy rainfall period. Clockwise circulation was indicated over the Pacific Ocean east of Japan owing to the upper-tropospheric low QGPV anomaly. Moreover, the lower-level cyclonic circulation over the Korean Peninsula was induced by the notably high QGPV anomaly in the upper troposphere (Fig. 8a), which may have partly contributed to the northeastward transport of moisture to Japan in the lower troposphere (Fig. 2b).

It is well known that surface heat transport is vital to baroclinic wave amplification and maintenance. The advection of surface temperature by the induced zonal geostrophic winds is shown in Fig. 8c. Since the summer background air temperature over the subtropical western Pacific has a westward positive gradient in the lower troposphere (Fig. 8b), the induced anomalous easterly wind advects cold air temperatures from the sea side. The cold air advection may contribute to the maintenance and enhancement of the NWPSH because surface cold anomalies behave as anticyclonic PV (Hoskins et al. 1985). This can be confirmed from Fig. 8d, which shows the streamfunction tendency at 1000 hPa only due to the upper-level-induced zonal temperature advection. The region of the positive streamfunction tendency coincided locally with that of the enhanced NWPSH (Fig. 2a), accompanied by a poleward tilting structure with height associated with the zonal heat transport. This structure is suitable for circulation anomalies over the summer subtropical western Pacific due to the westward positive air temperature gradient in the climatology, like as midlatitude baroclinic instability waves tilting westward with height due to the basic southward positive thermal gradient. In fact, the northward tilting structure of the circulation anomalies over the northwestern Pacific exhibited effective energy conversion to the perturbations (Kosaka and Nakamura 2006). These results suggest that the anticyclonic circulation anomaly in the upper troposphere over the western North Pacific acted to enhance and maintain the surface NWPSH through a baroclinic connection characterized by the northward-tilting structure.

Similarly, the strong relationship between the surface OH and upper-tropospheric blocking high over eastern Siberia can be found in Fig. 8c and d, which is consistent with Nakamura and Fukamachi (2004). This can also be identified in the anomalous circulation fields, in which the height axis tilted poleward with altitude around the Okhotsk Sea and eastern Siberia (Fig. 2a, c).

3.3 Role of tropical modulation in August 2021

3.3.1 Tropical heat forcing on the surface NWPSH

It is widely accepted that the modulation of tropical convective activity has great impacts on the NWPSH variability and subsequent precipitation variability in East Asia (e.g., Wang et al. 2000, 2013; Kosaka et al. 2013; Xie et al. 2016); however, previous studies have mainly focused on the Meiyu–Baiu season or the JJA mean fields. Therefore, using the LBM, we first confirm the area-wise contribution of the tropical heat forcing to the anomalous NWPSH in the basic state in late summer (August). Figure 9a shows the tropical heating contributions to the anomalous NWPSH as area-averaged surface pressure response to the solely imposed heating in each $10^\circ \times 10^\circ$ grid point over the Indo–Pacific sector, where the imposed heating has an idealized vertical

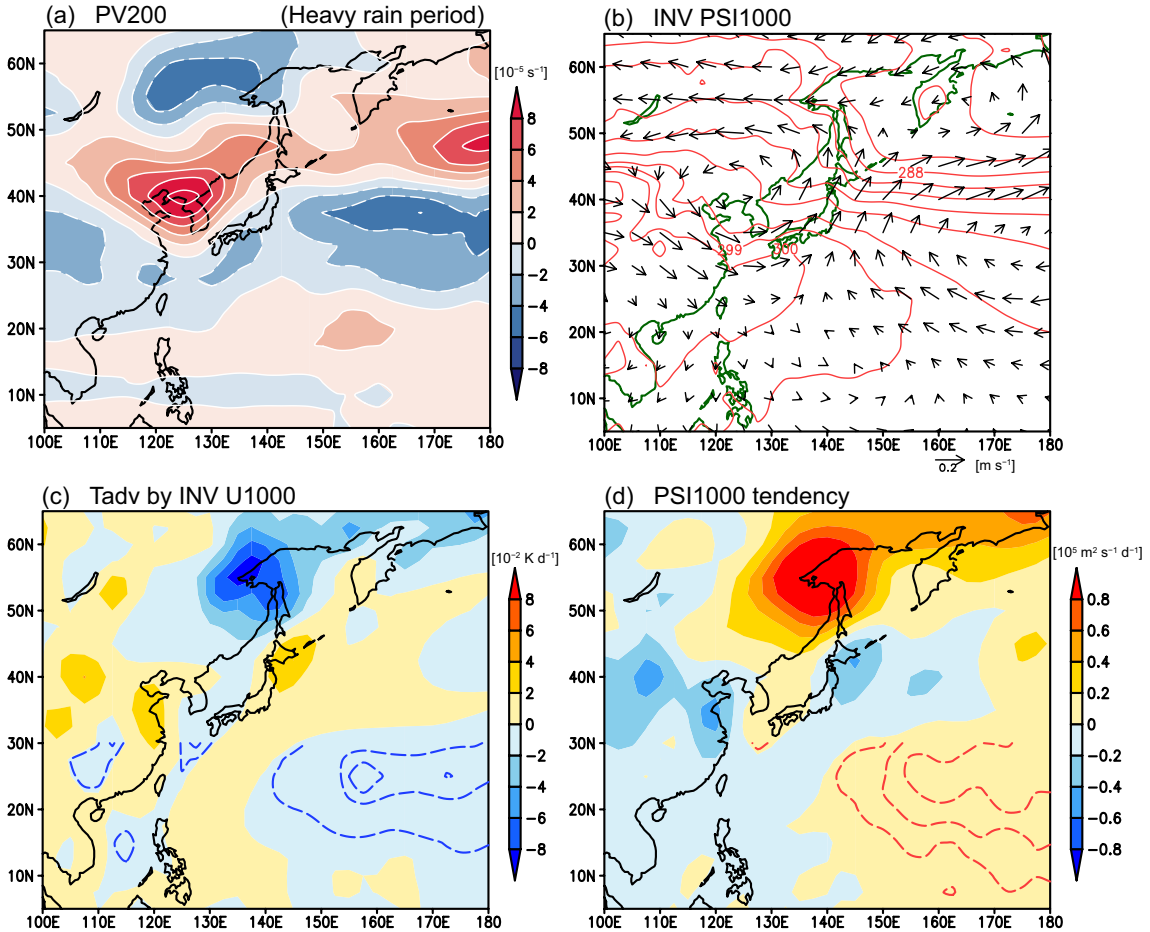

Fig. 8 QGPV inversion results. **a** QGPV anomaly at 200 hPa (unit: s^{-1}) during the heavy rainfall period. **b** Anomalous geostrophic winds at 1000 hPa (vectors; unit: m s^{-1}) solely induced by the PV anomalies at 200 hPa in the Northern Hemisphere. Climatological-mean air temperature at 1000 hPa (unit: K) is superimposed by red contours. **c** Air temperature advection (unit: K day^{-1}) by the induced anomalous zonal geostrophic winds at 1000 hPa. Blue contours secondarily indicate its −0.7, −0.5, and -0.1×10^{-2} K day^{-1} isolines in the south of 30°N. **d** Tendency of streamfunction at 1000 hPa (unit: m^2 s^{-1} day^{-1}) solely due to the air temperature advection by the induced anomalous zonal winds. Red contours secondarily indicate its 0.02, 0.05, and 0.1×10^5 m^2 s^{-1} day^{-1} isolines in the south of 30°N

structure with a maximum of ~1.7 K day^{-1} at $\sigma=0.45$, and the background state is the climatological-mean field in August derived from JRA-55. Overall, positive contributions were dominant over the Indian Ocean, whereas negative contributions were dominant over the tropical Pacific Ocean. The positive values over the tropical Indian Ocean indicate that anomalous heating intensified the NWPSH. This may be consistent with the Kelvin wave-induced Ekman divergence mechanism proposed by Xie et al. (2009), who showed that a warm equatorial Kelvin wave forced by Indian Ocean warming is responsible for the anomalous anticyclone and weakened rainfall over the subtropical northwestern Pacific by inducing atmospheric surface Ekman divergence. The contributions of the western Indian Ocean were slightly stronger than those of the eastern Indian Ocean. These results are suggestive of great potential to cause the enhanced NWPSH and resultant heavy rainfall in East Asia not only in the Meiyu–Baiu season but also in August from the viewpoint of the tropical Indian Ocean forcing. For the Pacific Ocean, negative values indicate the contribution of tropical anomalous cooling to the reinforcement of the NWPSH (Fig. 9a). In the equatorial lower troposphere, external atmospheric cooling may excite a pair of anticyclonic circulations on the western side, which is well known as the Rossby wave response in the Matsuno–Gill type heat-induced atmospheric response (Matsuno 1966; Gill 1980). Based on this idea, the diabatic cooling associated with suppressed convective activity over the equatorial central Pacific around the date line may remotely induce the enhancement of NWPSH. This mechanism appears to be consistent with the experimental results of Wang et al. (2013), who showed that La Niña-like SST cooling in the central Pacific may

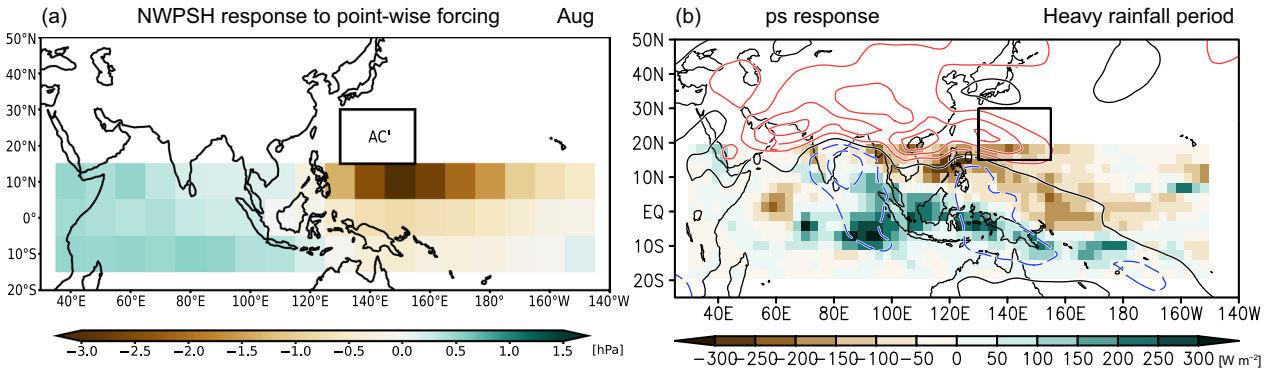

Fig. 9 The LBM experiment results. **a** Anomalous heating contribution to the development of NWPSH. Plotted values are area-averaged surface pressure anomaly in the subtropical northwestern Pacific [15°–30°N, 130°–155°E] (black rectangle) as a response to the idealized heating in each grid with the background state in August. Positive values in each grid indicate that the enhancement of convective activity strengthens the anomalous anticyclone (AC′) over the northwestern Pacific, and vice versa. **b** Steady response of surface pressure (contours; unit: hPa) to the prescribed heating anomalies over 20°S–20°N, 30°E–150°W during the heavy rainfall period. Red, blue, and black contours denote positive, negative, and zero values, respectively. The vertically integrated heat source anomaly from the surface to 10 hPa is indicated by shaded grid boxes (unit: W m^{-2})

be responsible for the stronger-than-normal NWPSH. Moreover, the striking local cooling contribution over the northwestern Pacific (10°N, 140°–170°E) is indicative of moist feedback between the atmospheric circulation and convective activity in the development and maintenance of the NWPSH. The locally suppressed convective activities strengthen the NWPSH; simultaneously, anomalous surface easterly winds on the southern flank of the anomalous anticyclone induce atmospheric Ekman divergence and suppress convection over the northwestern Pacific (Xie et al. 2009, 2016; Hu et al. 2019).

In August 2021, tropical convective modulation was characterized by enhancement over the eastern Indian Ocean and suppression over the tropical western–central Pacific (Fig. 1b). To assess the contribution of the tropical convection anomalies to the intensification of the NWPSH, we performed another set of sensitivity experiments for realistic external heat forcing using the LBM. In the experiments, the diabatic heating anomalies during the heavy rainfall period of August 2021, derived from JRA-55, were prescribed for the model. The imposed diabatic heat source (Q) was calculated as a residual of the thermodynamic equation, as follows (Yanai et al. 1973):

$$\frac{Q}{c_p} = \frac{\partial T}{\partial t} + \mathbf{v} \cdot \nabla T + \omega \left(\frac{\partial T}{\partial p} - \frac{RT}{c_p p} \right), \tag{7}$$

where $\mathbf{v}$ is the horizontal wind vector, ω is the vertical p-velocity, c_p is the specific heat for the dry air, and Q is the apparent heat source. The calculation was conducted based on the 6-hourly time step. As shown in Fig. 9b, the anomaly of the vertically integrated Q in the tropics was in good agreement with the observed precipitation anomaly (Fig. 1b), indicating the dominant role of precipitation in the heat source over the tropics. The heat source anomaly only across the region from the tropical Indian Ocean to the central Pacific [20°S–20°N, 30°E–150°W] was prescribed in the model as external forcing with the basic state as the climatological-mean field in August derived from JRA-55. The data were interpolated into the LBM grid.

Figure 9b shows the atmospheric response in the LBM to the diabatic heat source anomaly during the heavy rainfall period in August 2021. The surface pressure over the subtropical northwestern Pacific was anomalously high, indicating strengthening of the NWPSH due to the tropical heat forcing. Relatively low pressure over Japan was also represented in the model response. The full heating anomaly over the tropical Indo–western Pacific sector almost explains the intensification of the NWPSH, while one may wonder which is more important, the heating anomaly or the cooling anomaly. We further compared the contributions of the anomalous heating and cooling to the anomalous NWPSH by performing sensitivity experiments only for the positive and negative anomalies of the diabatic heat source, respectively. In the model responses (Additional file 1: Fig. S3), the anomalous heating (cooling) increased the surface pressure over the northern (southern) portion of the NWPSH region, which means that the spatial distributions of the atmospheric responses only to the anomalous heating/cooling were not entirely consistent with that of the reanalysis and full heating experiment. Therefore, these experimental results indicate that it is

a combination of the anomalous heating in the eastern Indian Ocean and the anomalous cooling in the tropical western Pacific that plays a crucial role in the intensification and localization of the surface NWPSH.

Meanwhile, we should note that the contribution of the tropical heat forcing during the August 2021 event may be evident only in the lower troposphere. The upper-tropospheric circulation response in the LBM experiment against the realistic heating anomalies exhibited a *cyclonic* (not anticyclonic) circulation anomaly over the subtropical northwestern Pacific due to the baroclinicity of the Matsuno–Gill type Rossby wave response (not shown), which completely differs from the observed tripolar structure of the anomalous circulation field. Thus, the tropical heat forcing mainly induced the SLP anomaly, and the extratropical variations also contributed to the surface circulation anomalies through the Rossby wave propagation in the upper troposphere and subsequent PV response. The coherent occurrence of the tropical heat forcing and extratropical variations was the essential factor for the occurrence of the heavy rainfall event in August 2021 from a climate system perspective.

3.3.2 Possible formation process of convective heating anomalies

The numerical experiment described in the previous subsection indicated the important roles of the combination effect of enhanced convective activity over the eastern Indian Ocean and suppression over the tropical Pacific in reinforcing the NWPSH. The tropical SST anomalies might contribute to the formation of the localized heating anomalies by promoting the anomalous convection because the distributions of the precipitation and SST anomalies within the tropics were regionally consistent as mentioned in Sect. 3.1 (Figs. 1b and 3a). However, the fact that the heavy rainfall prolonged only in August even though the tropical oceanic anomalies persisted throughout the summer of 2021 (Fig. 3b) suggests the importance of the intraseasonal variations inherent in the tropical–extratropical atmosphere. That is, the influence of the shorter timescale variability (< 1 month) in the atmosphere overlapped with that of the tropical oceanic anomalies varying in the longer timescale of more than several months, which resulted in the extremely heavy rainfall event. We finally provide a brief discussion about the formation process of the heat source anomalies in view of the tropical intraseasonal oscillation (ISO) of convective activity in this subsection.

Figure 10a shows the time–longitude cross section of the OLR and velocity potential anomalies in the tropics, which implies the eastward propagation of anomalous convective activity like the MJO (Madden and Julian 1972). The suppressed convective activity, found clearly in the positive anomaly of the velocity potential, began to propagate eastward from the western hemisphere in mid-July and subsequently reached the western Pacific (~ 150°E) during the heavy rainfall period in August. Moreover, the suppression was accompanied by the enhanced convective activity over the Indian Ocean (~ 60°–100°E), which appeared to propagate eastward faster than the suppressed convective activity. The phase transition of the MJO can also be found in the phase space diagram (Fig. 10b), indicating its approximately 40-day cycle. The MJO moved from weak phase 8 prior to the heavy rainfall event. Subsequently, it was amplified and remained in phase 2 during mid-August. Moreover, the ISO of convective activity can be identified as the BSISO, which dominates the ISO in the boreal summer and is characterized by a northeastward propagation over the northern Indian Ocean and western North Pacific (e.g., Wang and Xie 1997; Kemball-Cook and Wang 2001; Kikuchi 2020). The BSISO quickly changed from phase 8 to phase 3 in early August 2021 and maintained phase 3 during the heavy rainfall period (Fig. 10c), showing rapid amplification of the first principal component of the BSISO. Phase 2 of the MJO and phase 3 of the BSISO are characterized by enhanced convection over the eastern Indian Ocean paired with suppressed convection over the northwestern Pacific, accompanied by the anomalous anticyclone over the subtropical northwestern Pacific (Donald et al. 2006; Pai et al. 2011; Lee et al. 2013; Kikuchi 2021). This is consistent with our results on the August 2021 event. Thus, it is suggested that the ISO amplification and phase transition toward the tropical Indo–western Pacific Ocean sector may be responsible for the pair of convective activity anomalies over the eastern Indian Ocean and tropical western Pacific, which resulted in the intensification of the surface NWPSH and heavy rainfall in late summer.

4 Concluding remarks

In this study, large-scale atmospheric and oceanic fields during heavy rainfall over Japan in August 2021 and the related dynamic mechanisms were examined from a teleconnection perspective. The essential tropical and extratropical anomalies that resulted in the prolonged heavy rainfall are illustrated schematically in Fig. 11. During the heavy rainfall period, the atmospheric circulation field was characterized by the enhanced OH, Korean trough, and NWPSH, which were identified as a three-dimensional meridional tripolar structure of anomalous circulations. They have been proposed to be dynamically linked with each other through the following sequential mechanism: The surface OH was closely associated with the upper-level wave breaking over eastern Siberia and exhibited a northward tilt with height. South of

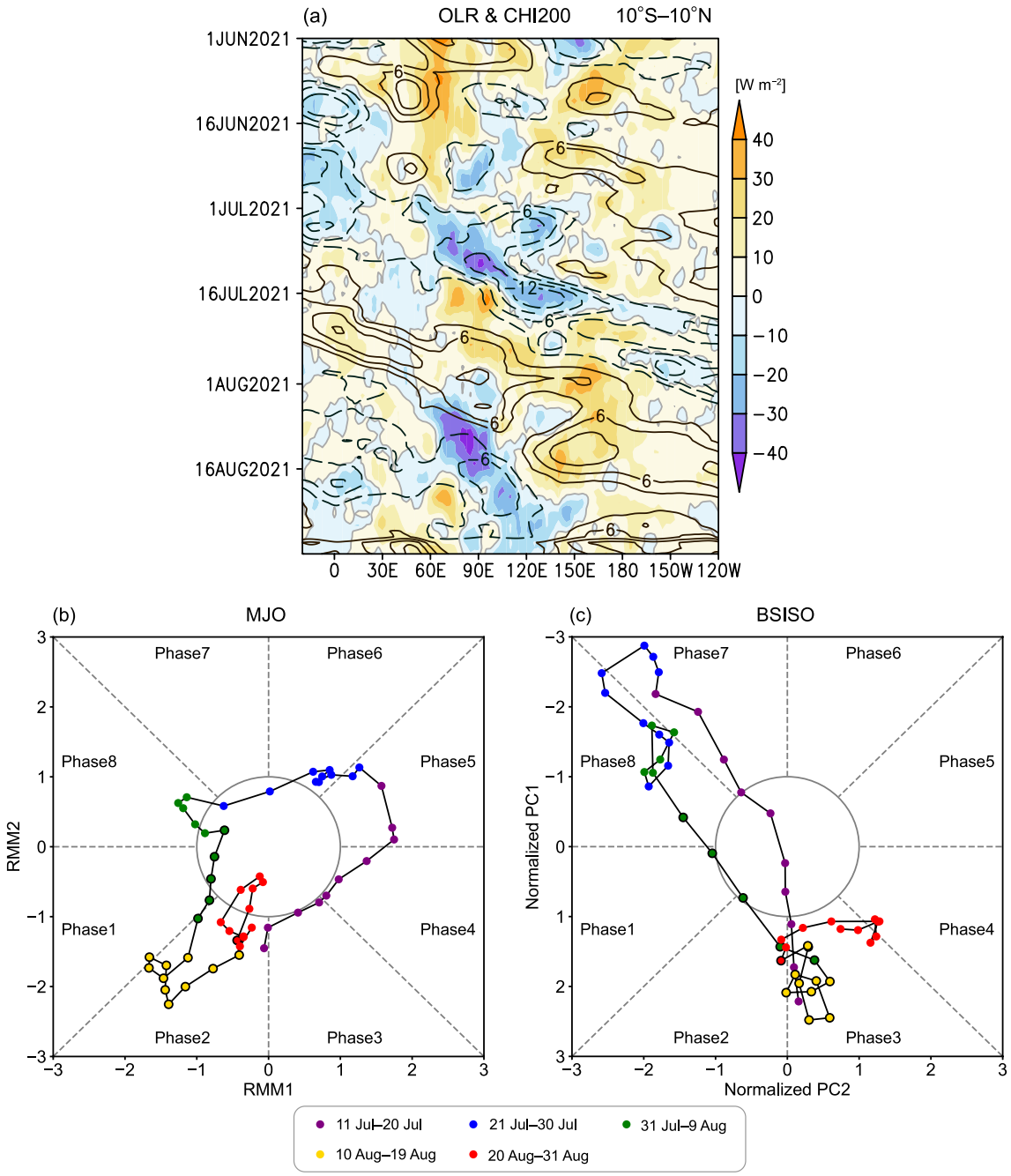

Fig. 10 **a** Time-longitude cross section of anomalies of OLR (shading; unit: W m^{-2}) and 200-hPa velocity potential (contours; unit: 10^6 m^2 s^{-1}) averaged in the tropics [10°S–10°N] from June 1 to August 31, 2021. A 5-day running mean was applied. The positive (negative) anomaly of velocity potential indicates anomalous convergence (divergence) of winds in the upper troposphere and the zero contours were omitted. **b**, **c** Phase space diagrams of MJO and BSISO, respectively, during the period of July 11–August 31, 2021 with an interval of 1 day. The dots enclosed by the black border line represent the heavy rainfall period [August 5–20, 2021]

the blocking high, synoptic depressions detected as cut-off lows or troughs intermittently moved and remained over the Korean Peninsula, which was important for strengthening the stationary Korean trough. Depression tracking analysis using the COL index revealed that one of the upper-level depressions was generated over central Siberia 11 days before the heavy rainfall peak. The stationary Korean trough and stagnated synoptic depressions were concurrent with the blocking high over eastern Siberia. Simultaneously, stationary Robby wave

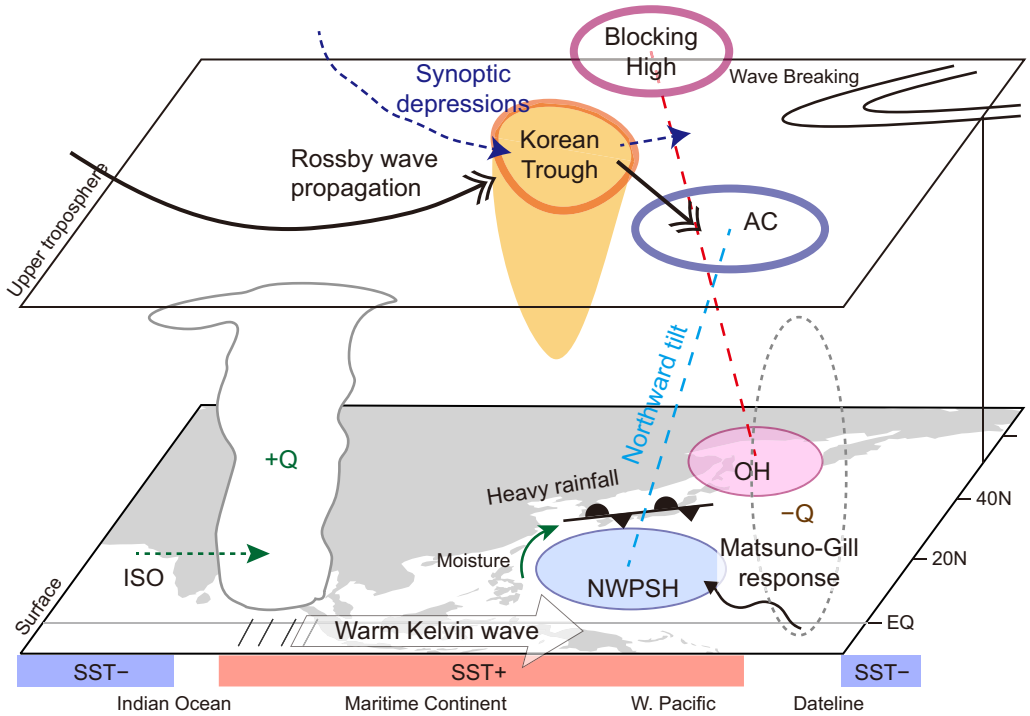

Fig. 11 Schematic illustration of predominant anomalies and mechanisms brought the prolonged heavy rainfall to Japan in August 2021

propagation from upstream may have contributed to the Korean trough. The southeastward Rossby wave emanating from the Korean trough further excited the anticyclonic circulation anomaly over the northwestern Pacific in the upper troposphere. This anomalous anticyclone may have afforded the enhancement and maintenance of the surface NWPSH, which exhibited a northward-tilting structure with height due to the background zonal temperature gradient over the northwestern Pacific. These results suggest that the meridional tripolar circulation anomalies were dynamically correlated, and their coherent amplification brought record heavy rainfall to Japan through increased moisture transport, convergence, and dynamically induced ascent.

Furthermore, the pair of reinforced tropical convection over the eastern Indian Ocean and suppressed convection over the tropical western–central Pacific intensified the NWPSH (Fig. 11). The diabatic heating contribution over the eastern Indian Ocean may be associated with the warm equatorial Kelvin wave accompanied by the surface Ekman divergence off the equator, whereas the anomalous cooling over the tropical central Pacific can be understood as the Matsuno–Gill type heat-induced atmospheric response. The suppressed convective activity over the tropical western Pacific may involve the local convection–circulation feedback with the NWPSH. The tropical oceanic anomalies characterized by the negative-phase IOD and multi-year La Niña, that can promote the anomalous convection, persisted throughout the summer of 2021. Moreover, the anomalous convective activity was closely associated with the phase transition and amplification of the tropical ISO over the Indo–western Pacific Ocean sector, resulting in the intensified NWPSH and heavy rainfall. The simultaneous occurrence of intraseasonal convective modulations in the tropics and the dynamically correlated tripolar structure of anomalous circulations in the extratropics can be regarded as key factors resulting in the heavy and prolonged rainfall in August 2021.

From the ENSO and IPOC perspectives, it is controversial that heavy rainfall in August 2021 occurred under multi-year La Niña conditions. The NWPSH tends to be stronger in the post-El Niño summer, which is associated with the capacitor effect of the Indian Ocean (e.g., Xie et al. 2009, 2016). Indeed, Naoi et al. (2020) showed the weakening of the NWPSH and the resultant decrease in the occurrence frequency of atmospheric rivers in the vicinity of Japan during the La Niña summer continued from the preceding-winter La Niña. Furthermore, previous studies indicated the warmer conditions in Japan and dry conditions in central-eastern China during the summer between the wintertime maturity of multi-year La Niña (Ueda and Kawamura 2004; Iwakiri and Watanabe 2020; Huang et al. 2022). These previous indications, as well as

our results, suggest that the highlighted effects of the tropical ISO, IOD, and extratropical tripolar structure consisting of the OH/blocking, Korean trough, and NWPSH were prioritized over the tropical Pacific SST forcing in the August 2021 event.

Although this study attempted to clarify the dynamic relationship of the circulation pattern by focusing on an extreme event, we plan to verify whether the synchronicity mechanism shown in this study occurs in other heavy and prolonged rainfall events as well. In recent summers, disastrous heavy rainfall associated with stagnated rain fronts has occurred over East Asia approximately every year, such as in July 2018 (e.g., Shimpo et al. 2019), June–July 2020 (e.g., Ueda et al. 2021; Horinouchi et al. 2021), August 2021 (this study), and August 2022 (JMA 2022). This may be related to the 2–3- and 3–5-year oscillations in the NWPSH (Sui et al. 2007; Wu and Zhou 2008; Chung et al. 2011) as well as to the anthropogenic global warming. The heavy rainfall event in August 2021, which was associated with the stagnated Baiu-like rain front (Fig. 1), can be referred to as a "re-appearance" of the Baiu front in late summer. Baiu has been interpreted in view of the seasonal evolution of the Asian monsoon (Kawamura and Murakami 1998; Ueda et al. 2009), and the transition of climatological fields from the preceding season to the fall rainfall season (Akisame in Japanese) should be analyzed to further understand the re-appearance of the Baiu front and its relationship/difference with the Akisame front.

Abbreviations

AS	Average slope
BSISO	Boreal summer intraseasonal oscillation
COL	Cutoff low
ENSO	El Niño–Southern oscillation
IOD	Indian ocean dipole
IPOC	Indo–western Pacific Ocean capacitor
ISO	Intraseasonal oscillation
JMA	Japan Meteorological Agency
LBM	Linear baroclinic model
MJO	Madden–Julian oscillation
NWPSH	Northwestern Pacific subtropical high
OH	Okhotsk high
PV	Potential vorticity
QG	Quasi-geostrophic
SST	Sea surface temperature

Supplementary Information

The online version contains supplementary material available at https://doi.org/10.1186/s40645-023-00598-4.

Additional file 1. Fig. S1. Vertically integrated *Q*-vectors and their divergence in August 11–15, 2021. **Fig. S2.** Snapshots of spatial distributions of AS^+ at 200 and 500 hPa from 00 UTC 10 to 12 UTC on August 14, 2021 with 12-h intervals. **Fig. S3**. Atmospheric responses to the tropical positive and negative heat-source anomalies in the LBM.

Acknowledgements

The authors are grateful to Dr. Satoru Kasuga for providing the COL index data and exciting discussion, and to Mr. Shunsuke Hashimoto for his assistance in our LBM experiments. We would also like to thank the two anonymous reviewers for providing constructive comments on an earlier version of this paper.

Author contributions

MK, HU, MH, and KT conceived and designed the study. MK analyzed the data, performed the experimental study, created the figures, and wrote the manuscript. MH provided the COL index data and KT provided the code for QGPV inversion, respectively, to the corresponding author. HU, TI, MH, and KT helped in the interpretation of the results and the construction of the manuscript. All the authors have read and approved the final version of the manuscript.

Funding

This work was supported by JSPS KAKENHI (grant number 21H00626).

Availability of data and materials

The JRA-55 dataset, COBE-SST, and AMeDAS are provided by the JMA (https://jra.kishou.go.jp/JRA-55/index_en.html; https://ds.data.jma.go.jp/tcc/tcc/index.html; https://www.jma.go.jp/jma/index.html). The GPCP data are provided at NOAA NCEI (https://www.ncei.noaa.gov/) and OLR data are provided at NOAA PSL (https://psl.noaa.gov/). The RMM data are available at http://www.bom.gov.au/climate/enso/#tabs=Tropics&tropics=History-to-now, and the BSISO index is available at https://www.apcc21.org/ser/moni.do?lang=en#grap1. Documents and codes for the LBM are available at https://ccsr.aori.u-tokyo.ac.jp/~lbm/sub/lbm.html.

Declarations

Competing interests

The authors declare that they have no competing interest.

Author details

[1]Graduate School of Science and Technology, University of Tsukuba, 1-1-1 Tennodai, Tsukuba, Ibaraki 305-8572, Japan. [2]Faculty of Life and Environmental Sciences, University of Tsukuba, 1-1-1 Tennodai, Tsukuba, Ibaraki 305-8572, Japan. [3]Faculty of Science, Niigata University, 8050 Ikarashi 2-no-cho, Nishi-Ku, Niigata 950-2181, Japan. [4]Department of Astrophysics and Atmospheric Sciences, Faculty of Science, Kyoto Sangyo University, Motoyama, Kita-Ku, Kyoto, Kamigamo 603-8555, Japan.

Received: 22 June 2023 Accepted: 7 November 2023
Published online: 06 December 2023

References

Abatzoglou JT, Magnusdottir G (2006) Planetary wave breaking and nonlinear reflection: seasonal cycle and interannual variability. J Clim 19:6139–6152

Akiyama T (1973) The large-scale aspect of the characteristic features of the Baiu front. Pap Meteor Geophy 24:157–188

Barriopedro D, García-Herrera R, Lupo AR, Hernández E (2006) A climatology of Northern hemisphere blocking. J Clim 19:1042–1063

Bretherton FP (1966) Critical layer instability in baroclinic flows. Quart J Roy Meteor Soc 92:325–334

Chang CP, Zhang Y, Li T (2000) Interannual and interdecadal variations of the East Asian summer monsoon and tropical Pacific SSTs. Part I: roles of the subtropical ridge. J Clim 13:4310–4325

Charney JG, Stern ME (1962) On the stability of internal baroclinic jets in a rotating atmosphere. J Atmos Sci 19:159–172

Chen G, Huang R (2012) Excitation mechanisms of the teleconnection patterns affecting the July precipitation in Northwest China. J Clim 25:7834–7851

Chen X, Wen Z, Song Y, Guo Y (2022) Causes of extreme 2020 Meiyu-Baiu rainfall: a study of combined effect of Indian Ocean and Arctic. Clim Dyn 59:3485–3501
Chowdary JS, Gnanaseelan C, Chakravorty S (2013) Impact of Northwest Pacific anticyclone on the Indian summer monsoon region. Theor Appl Climatol 113:329–336
Chung PH, Sui CH, Li T (2011) Interannual relationships between the tropical sea surface temperature and summertime subtropical anticyclone over the western North Pacific. J Geophys Res 116:D13111. https://doi.org/10.1029/2010JD015554
Donald A, Meinke H, Power B, de HN Maia A, Wheeler MC, White N, Stone RC, Ribbe J, (2006) Near-global impact of the Madden–Julian oscillation on rainfall. Geophys Res Lett 33:L09704. https://doi.org/10.1029/2005GL025155
Du Y, Xie SP, Huang G, Hu K (2009) Role of air–sea interaction in the long persistence of El Niño–induced North Indian ocean warming. J Clim 22:2023–2038
Enomoto T (2004) Interannual variability of the Bonin high associated with the propagation of Rossby waves along the Asian jet. J Meteor Soc Japan 82:1019–1034
Enomoto T, Hoskins BJ, Matsuda Y (2003) The formation mechanism of the Bonin high in August. Quart J Roy Meteor Soc 129:157–178
Gill AE (1980) Some simple solutions for heat-induced tropical circulation. Quart J Roy Meteor Soc 106:447–462
Harada Y, Endo H, Takemura K (2020) Characteristics of large-scale atmospheric fields during heavy rainfall events in western Japan: comparison with an extreme event in early July 2018. J Meteor Soc Japan 98:1207–1229
Hirota N, Takahashi M (2012) A tripolar pattern as an internal mode of the East Asian summer monsoon. Clim Dyn 39:2219–2238
Holton JR (1992) An introduction to dynamic meteorology. 3rd edition. Academic Press
Horinouchi T, Kosaka Y, Nakamigawa H, Nakamura H, Fujikawa N, Takayabu YN (2021) Moisture supply, jet, and silk-road wave train associated with the prolonged heavy rainfall in Kyushu, Japan in early July 2020. SOLA 17B:1–8
Hoskins BJ, Draghici I, Davies HC (1978) A new look at the ω-equation. Quart J Roy Meteor Soc 104:31–38
Hoskins BJ, McIntyre ME, Robertson AW (1985) On the use and significance of isentropic potential vorticity maps. Quart J Roy Meteor Soc 111:877–946
Hu K, Huang G, Xie SP, Long SM (2019) Effect of the mean flow on the anomalous anticyclone over the Indo-Northwest Pacific in post-El Niño summers. Clim Dyn 53:5725–5741
Huang G, Wang R, Liu J, Gao L, Liu M, Chen Q (2022) Seasonally evolving impacts of multiyear La Niña on precipitation in southern China. Front Earth Sci 10:884604. https://doi.org/10.3389/feart.2022.884604
Huffman GJ, Adler RF, Morrissey MM, Bolvin DT, Curtis S, Joyce R, McGavock B, Susskind J (2001) Global precipitation at one-degree daily resolution from multisatellite observations. J Hydrometeorol 2:36–50
Ishii M, Shouji A, Sugimoto S, Matsumoto T (2005) Objective analyses of sea surface temperature and marine meteorological variables for the 20th century using ICOADS and the Kobe collection. Int J Climatol 25:865–879
Iwakiri T, Watanabe M (2020) Multiyear La Niña impact on summer temperature over Japan. J Meteor Soc Japan 98:1245–1260
JMA (2021) Press release "climate characteristics and factors behind record-heavy rain in Japan in Aug 2021". https://www.data.jma.go.jp/tcc/tcc/news/press_20210924.pdf. Accessed 30 Sep 2023
JMA (2022) Press release "climate characteristics and factors behind record-high temperatures in late June/early July 2022 and subsequent weather conditions". https://www.data.jma.go.jp/tcc/tcc/news/press_20220914.pdf. Accessed 30 Sep 2023
Ju J, Slingo J (1995) The Asian summer monsoon and ENSO. Quart J Roy Meteor Soc 121:1133–1168
Kamae Y, Mei W, Xie SP, Naoi M, Ueda H (2017) Atmospheric rivers over the northwestern Pacific: climatology and interannual variability. J Clim 30:5605–5619
Kasuga S, Honda M, Ukita J, Yamane S, Kawase H, Yamazaki A (2021) Seamless detection of cutoff lows and preexisting troughs. Mon Wea Rev 149:3119–3134
Kawamura R, Murakami T (1998) Baiu near Japan and its relation to summer monsoons over Southeast Asia and the western North Pacific. J Meteor Soc Japan 76:619–639
Kawamura R, Matsuura T, Iizuka S (2001) Interannual atmosphere-ocean variations in the tropical western North Pacific relevant to the Asian summer monsoon-ENSO coupling. J Meteor Soc Japan 79:883–898
Kawasaki K, Tachibana Y, Nakamura T, Yamazaki K (2021) Role of the cold Okhotsk sea on the climate of the North Pacific subtropical high and Baiu precipitation. J Clim 34:495–507
Kemball-Cook S, Wang B (2001) Equatorial waves and air-sea interaction in the boreal summer intraseasonal oscillation. J Clim 14:2923–2942
Kikuchi K (2020) Extension of the bimodal intraseasonal oscillation index using JRA-55 reanalysis. Clim Dyn 54:919–933
Kikuchi K (2021) The boreal summer intraseasonal oscillation: a review. J Meteor Soc Jpn 99:933–972
Kobayashi S, Ota Y, Harada Y, Ebita A, Moriya M, Onoda H, Onogi K, Kamahori H, Kobayashi C, Endo H, Miyaoka K, Takahashi K (2015) The JRA-55 reanalysis: general specifications and basic characteristics. J Meteor Soc Jpn 93:5–48
Kosaka Y, Nakamura H (2006) Structure and dynamics of the summertime Pacific-Japan teleconnection pattern. Quart J Roy Meteor Soc 132:2009–2030
Kosaka Y, Nakamura H, Watanabe M, Kimoto M (2009) Analysis on the dynamics of a wave-like teleconnection pattern along the summertime Asian jet based on a reanalysis dataset and climate model simulations. J Meteor Soc Jpn 87:561–580
Kosaka Y, Xie SP, Nakamura H (2011) Dynamics of interannual variability in summer precipitation over East Asia. J Clim 24:5435–5453
Kosaka Y, Xie SP, Lau NC, Vecchi GA (2013) Origin of seasonal predictability for summer climate over the northwestern Pacific. Proc Natl Acad Sci USA 110:7574–7579
Lee JY, Wang B, Wheeler MC, Fu X, Waliser DE, Kang IS (2013) Real-time multivariate indices for the boreal summer intraseasonal oscillation over the Asian summer monsoon region. Clim Dyn 40:493–509
Lejenäs H, Økland H (1983) Characteristics of northern hemisphere blocking as determined from long time series of observational data. Tellus 35A:350–362
Liebmann B, Smith CA (1996) Description of a complete (interpolated) outgoing longwave radiation dataset. Bull Amer Meteor Soc 77:1275–1277
Lu R (2001) Interannual variability of the summertime North Pacific subtropical high and its relation to atmospheric convection over the warm pool. J Meteor Soc Jpn 79:771–783
Madden RA, Julian PR (1972) Description of global-scale circulation cells in the tropics with a 40–50 day period. J Atmos Sci 29:1109–1123
Matsuno T (1966) Quasi-geostrophic motions in the equatorial area. J Meteor Soc Jpn 44:25–43
Nakamura H, Fukamachi T (2004) Evolution and dynamics of summertime blocking over the far east and the associated surface Okhotsk high. Quart J Roy Meteor Soc 130:1213–1233
Nakamura H, Nakamura M, Anderson JL (1997) The role of high- and low-frequency dynamics in blocking formation. Mon Wea Rev 125:2074–2093
Naoi M, Kamae Y, Ueda H, Mei W (2020) Impacts of seasonal transitions of ENSO on atmospheric river activity over East Asia. J Meteor Soc Japan 98:655–668
Ninomiya K, Mizuno H (1985) Anomalously cold spell in summer over northeastern Japan caused by northeasterly wind from polar maritime airmass. Part 2. structure of the northeasterly flow from polar maritime airmass. J Meteor Soc Japan 63:859–871
Ninomiya K, Shibagaki Y (2007) Multi-scale features of the Meiyu-Baiu front and associated precipitation systems. J Meteor Soc Jpn 85:103–122
Nitta T (1987) Convective activities in the tropical western Pacific and their impact on the Northern hemisphere summer circulation. J Meteor Soc Jpn 65:373–390
Nitta T (1990) Unusual summer weather over Japan in 1988 and its relationship to the tropics. J Meteor Soc Jpn 68:575–588
Paek H, Yu JY, Zheng F, Lu MM (2019) Impacts of ENSO diversity on the western Pacific and North Pacific subtropical highs during boreal summer. Clim Dyn 52:7153–7172

Pai DS, Bhate J, Sreejith OP, Hatwar HR (2011) Impact of MJO on the intraseasonal variation of summer monsoon rainfall over India. Clim Dyn 36:41–55
Park C, Son SW, Kim H, Ham YG, Kim J, Cha DH, Chang EC, Lee G, Kug JS, Lee WS, Lee YY, Lee HC, Lim B (2021a) Record-breaking summer rainfall in South Korea in 2020: synoptic characteristics and the role of large-scale circulations. Mon Wea Rev 149:3085–3100
Park C, Son SW, Kim JH (2021b) Role of baroclinic trough in triggering vertical motion during summertime heavy rainfall events in Korea. J Atmos Sci 78:1687–1702
Postel GA, Hitchman MH (1999) A climatology of Rossby wave breaking along the subtropical tropopause. J Atmos Sci 56:359–373
Rex DF (1950) Blocking action in the middle troposphere and its effect upon regional climate. I. An aerological study of blocking action. Tellus 2:196–211
Saji NH, Goswami BN, Vinayachandran PN, Yamagata T (1999) A dipole mode in the tropical Indian Ocean. Nature 401:360–363
Sampe T, Xie SP (2010) Large-scale dynamics of the Meiyu-Baiu rainband: environmental forcing by the westerly jet. J Clim 23:113–134
Sato N, Takahashi M (2006) Dynamical processes related to the appearance of quasi-stationary waves on the subtropical jet in the midsummer Northern hemisphere. J Clim 19:1531–1544
Sato N, Takahashi M (2007) Dynamical processes related to the appearance of the Okhotsk high during early midsummer. J Clim 20:4982–4994
Sekizawa S, Miyasaka T, Nakamura H, Shimpo A, Takemura K, Maeda S (2019) Anomalous moisture transport and oceanic evaporation during a torrential rainfall event over western Japan in early July 2018. SOLA 15A:25–30
Shimpo A, Takemura K, Wakamatsu S, Togawa H, Mochizuki Y, Takekawa M, Tanaka S, Yamashita K, Maeda S, Kurora R, Murai H, Kitabatake N, Tsuguti H, Mukougawa H, Iwasaki T, Kawamura R, Kimoto M, Takayabu I, Takayabu YN, Tanimoto Y, Hirooka T, Masumoto Y, Watanabe M, Tsuboki K, Nakamura H (2019) Primary factors behind the heavy rain event of July 2018 and the subsequent heat wave in Japan. SOLA 15A:13–18
Sui CH, Chung PH, Li T (2007) Interannual and interdecadal variability of the summertime western North Pacific subtropical high. Geophys Res Lett 34:L11701. https://doi.org/10.1029/2006GL029204
Tachibana Y, Iwamoto T, Ogi M, Watanabe Y (2004) Abnormal meridional temperature gradient and its relation to the Okhotsk high. J Meteor Soc Jpn 82:1399–1415
Takaya Y, Ishikawa I, Kobayashi C, Endo H, Ose T (2020) Enhanced Meiyu-Baiu rainfall in early summer 2020: aftermath of the 2019 super IOD event. Geophys Res Lett. https://doi.org/10.1029/2020GL090671
Takaya K, Nakamura H (2001) A formulation of a phase-independent wave-activity flux for stationary and migratory quasigeostrophic eddies on a zonally varying basic flow. J Atmos Sci 58:608–627
Takaya K, Nakamura H (2005) Mechanisms of intraseasonal amplification of the cold Siberian high. J Atmospheric Sci 62:4423–4440
Takemura K, Wakamatsu S, Togawa H, Shimpo A, Kobayashi C, Maeda S, Nakamura H (2019) Extreme moisture flux convergence over western Japan during the heavy rain event of July 2018. SOLA 15A:49–54
Terao T, Kubota T (2005) East-west SST contrast over the tropical oceans and the post El Niño western North Pacific summer monsoon. Geophys Res Lett 32:L15706. https://doi.org/10.1029/2005GL023010
Tomita T, Yoshikane T, Yasunari T (2004) Biennial and lower-frequency variability observed in the early summer climate in the western North Pacific. J Clim 17:4254–4266
Trenberth KE (1997) The definition of El Niño. Bull Amer Meteor Soc 78:2771–2777
Tsuji H, Yokoyama C, Takayabu YN (2020) Contrasting features of the July 2018 heavy rainfall event and the 2017 Northern Kyushu rainfall event in Japan. J Meteor Soc Japan 98:859–876
Ueda H, Kawamura R (2004) Summertime anomalous warming over the mid-latitude western North Pacific and its relationships to the modulation of the Asian monsoon. Int J Climatol 24:1109–1120
Ueda H, Ohba M, Xie SP (2009) Important factors for the development of the Asian-Northwest Pacific summer monsoon. J Clim 22:649–669
Ueda H, Yokoi M, Kuramochi M (2021) Enhanced subtropical anticyclone over the Indo-Pacific ocean associated with stagnation of the Meiyu-Baiu rainband during summer, 2020. SOLA 17B:14–18
Wakabayashi S, Kawamura R (2004) Extraction of major teleconnection patterns possibly associated with the anomalous summer climate in Japan. J Meteor Soc Japan 82:1577–1588
Wang B, Xie X (1997) A model for the boreal summer intraseasonal oscillation. J Atmos Sci 54:72–86
Wang B, Wu R, Fu X (2000) Pacific-east Asian teleconnection: how does ENSO affect East Asian climate? J Clim 13:1517–1536
Wang B, Wu R, Lau KM (2001) Interannual variability of the Asian summer monsoon: contrasts between the Indian and the western North Pacific-East Asian monsoons. J Clim 14:4073–4090
Wang B, Xiang B, Lee JY (2013) Subtropical high predictability establishes a promising way for monsoon and tropical storm predictions. Proc Natl Acad Sci USA 110:2718–2722
Watanabe M, Kimoto M (2000) Atmosphere-ocean thermal coupling in the North Atlantic: a positive feedback. Quart J Roy Meteor Soc 126:3343–3369
Webster PJ, Yang S (1992) Monsoon and ENSO: selectively interactive systems. Quart J Roy Meteor Soc 118:877–926
Wheeler MC, Hendon HH (2004) An all-season real-time multivariate MJO index: development of an index for monitoring and prediction. Mon Wea Rev 132:1917–1932
World meteorological organization (2022) WMO El Niño/La Niña Updates. https://community.wmo.int/activity-areas/climate/wmo-el-ninola-nina-updates. Accessed 30 Dec 2022
Wu B, Zhou T (2008) Oceanic origin of the interannual and interdecadal variability of the summertime western Pacific subtropical high. Geophys Res Lett 35:L13701. https://doi.org/10.1029/2008GL034584
Xie SP, Hu KM, Hafner J, Tokinaga H, Du Y, Huang G, Sampe T (2009) Indian ocean capacitor effect on Indo–western Pacific climate during the summer following El Niño. J Clim 22:730–747
Xie SP, Kosaka Y, Du Y, Hu KM, Chowdary JS, Huang G (2016) Indo-western Pacific ocean capacitor and coherent climate anomalies in post-ENSO summer: a review. Adv Atmos Sci 33:411–432
Yamazaki A, Itoh H (2013a) Vortex–vortex interactions for the maintenance of blocking. Part I: the selective absorption mechanism and a case study. J Atmos Sci 70:725–742
Yamazaki A, Itoh H (2013b) Vortex–vortex interactions for the maintenance of blocking. Part II: numerical experiments. J Atmos Sci 70:743–766
Yanai M, Esbensen S, Chu JH (1973) Determination of bulk properties of tropical cloud clusters from large-scale heat and moisture budgets. J Atmos Sci 30:611–627
Yang J, Liu Q, Xie SP, Liu Z, Wu L (2007) Impact of the Indian ocean SST basin mode on the Asian summer monsoon. Geophys Res Lett 34:L02708. https://doi.org/10.1029/2006GL028571
Yim SY, Wang B, Xing W (2014) Prediction of early summer rainfall over South China by a physical-empirical model. Clim Dyn 43:1883–1891
Yokoyama C, Tsuji H, Takayabu YN (2020) The effects of an upper-tropospheric trough on the heavy rainfall event in July 2018 over Japan. J Meteor Soc Japan 98:235–255
Yoshino MM (1965) Four stages of the rainy season in early summer over East Asia (Part I). J Meteor Soc Jpn 43:231–245
Zhao S, Sun J (2007) Study on cut-off low-pressure systems with floods over Northeast Asia. Meteorol Atmos Phys 96:159–180

Publisher's Note